Naval Research Laboratory

Washington, DC 20375-5320

Channel Spread Parameters for the High-Latitude, Near-Vertical-Incidence-Skywave HF Channel: Correlation with Geomagnetic Activity

L. S. WAGNER
J. A. GOLDSTEIN

Center for Computer High Assurance Systems
Information Technology Division

July 13, 1995

REPORT DOCUMENTATION PAGE

Public reporting burden for this collection of information is estimated to average 1 hour per response, including the time for reviewing instructions, searching existing data sources, gathering and maintaining the data needed, and completing and reviewing the collection of information. Send comments regarding this burden estimate or any other aspect of this collection of information, including suggestions for reducing this burden, to Washington Headquarters Services, Directorate for Information Operations and Reports, 1215 Jefferson Davis Highway, Suite 1204, Arlington, VA 22202-4302, and to the Office of Management and Budget, Paperwork Reduction Project (0704-0188), Washington, DC 20503.

1. AGENCY USE ONLY (Leave Blank)	2. REPORT DATE July 13, 1995	3. REPORT TYPE AND DATES COVERED Final — May to July 1988	
4. TITLE AND SUBTITLE Channel Spread Parameters for the High-Latitude, Near-Vertical-Incidence-Skywave HF Channel: Correlation with Geomagnetic Activity			5. FUNDING NUMBERS PE - 61153N PR - LR033-02-44
6. AUTHOR(S) L. S. Wagner and J. A. Goldstein			
7. PERFORMING ORGANIZATION NAME(S) AND ADDRESS(ES) Naval Research Laboratory Washington, DC 20375-5320			8. PERFORMING ORGANIZATION REPORT NUMBER NRL/FR/5550--95-9772
9. SPONSORING/MONITORING AGENCY NAME(S) AND ADDRESS(ES) Office of Naval Research 800 North Quincy Street Arlington, VA 22217-5660			10. SPONSORING/MONITORING AGENCY REPORT NUMBER

11. SUPPLEMENTARY NOTES

12a. DISTRIBUTION/AVAILABILITY STATEMENT Approved for public release; distribution unlimited.	12b. DISTRIBUTION CODE

13. ABSTRACT (Maximum 200 words)

Results of measurements on a high-latitude, near-vertical-incidence, HF skywave channel are presented. The measurements are for a time period (May 1988), roughly two years after the peak of solar cycle #22, when the mean sunspot number was 85. The measurement periods include day, afternoon, night, and early morning times and cover a wide range of geomagnetic disturbance conditions. Signal amplitude, delay-spread and Doppler-spread are the channel characteristics of primary interest. The correlation of these channel characteristics with geomagnetic activity and with the position of the propagation path relative to selected regions of the auroral zone are examined. Ionogram characteristics for all measurements are briefly reviewed in light of geomagnetic and geographic factors. Four selected cases, representative of magnetically quiet daytime conditions, magnetically active daytime conditions, magnetically quiet nighttime conditions, and magnetically active nighttime conditions are examined in detail. The measurement results indicate that, depending on geomagnetic and geographic factors, the received signals may be the result of simple reflection from a smoothly varying ionosphere, multipath reflection from an irregular ionosphere, or scattering (or a combination of multipath reflection and scattering) from an irregular ionosphere. Signals for the four groups are shown to be readily distinguishable on the basis of their characteristics and provide an estimate of the range of values of Doppler-spread and spread-factor that may be expected on the channel.

14. SUBJECT TERMS		15. NUMBER OF PAGES
High-latitude, high-frequency skywave propagation Auroral zone ionosphere Geomagnetic disturbances Radio channel characteristics		54
		16. PRICE CODE

17. SECURITY CLASSIFICATION OF REPORT UNCLASSIFIED	18. SECURITY CLASSIFICATION OF THIS PAGE UNCLASSIFIED	19. SECURITY CLASSIFICATION OF ABSTRACT UNCLASSIFIED	20. LIMITATION OF ABSTRACT UL

CONTENTS

CHANNEL SPREAD PARAMETERS FOR THE HIGH-LATITUDE, NEAR-VERTICAL-INCIDENCE-SKYWAVE HF CHANNEL: CORRELATION WITH GEOMAGNETIC ACTIVITY

1. INTRODUCTION

This report describes channel measurements made on a high-latitude, near-vertical-incidence, HF skywave channel. Because the high-latitude regions are more frequently and more severely disturbed than are the middle- and equatorial-latitude regions, they present a special challenge to high-frequency (HF) radio systems. The high-latitude channel can be subdivided into three main regions: the polar cap, the auroral oval,[*] and the high-latitude region lying equatorward of the auroral oval (hereafter referred to as the subauroral region). The subauroral region includes the daytime diffuse auroral region and the nighttime ionospheric trough region. The location of these measurements (Fairbanks, Alaska) was selected because its latitude places it in proximity to the auroral oval.

The primary focus of this investigation is the one-hop F2 (1F2) near-vertical-incidence-skywave (NVIS) HF radio channel. The channel parameters of primary concern are signal amplitude, delay-spread, Doppler-spread, and channel spread factor. These parameters are all derivable from the channel scattering function (Bello 1963; Stein 1987). Signal amplitude is defined here as the peak value of the channel scattering function, in decibels, measured relative to an arbitrary but fixed reference. The delay-spread and Doppler-spread parameters are each expressed in terms of a "2σ" value, which is defined as twice the rms spread of delay or Doppler shift about its mean value. The channel spread factor is defined as the product of the 2σ values of the delay- and Doppler-spreads. Other factors that are considered, but are not the main subject of this report, include the characteristics of the sporadic E channel and the conditions under which blanketing sporadic E and enhanced auroral absorption are observed.

Channel conditions are expected to be most formidable at dusk and at night. Magnetically quiet daytime periods are usually characterized by a strong and frequently dominant F1 layer (Bates and Hunsucker 1974) that causes enhanced delay and delay dispersion of the F2 layer return, but does not otherwise seriously impede HF communication. As is demonstrated in this report, magnetically disturbed daytime conditions may be accompanied by disruptive effects on the channel such as enhanced absorption, caused by enhanced D layer ionization, and signal multipath and scatter, caused by irregularities in the ionospheric F layer (spread F).

Channel parameters are evaluated for a range of conditions including (1) optimal daytime conditions, (2) magnetically disturbed daytime conditions, (3) magnetically quiet nighttime conditions, and (4) magnetically disturbed nighttime conditions. The cases considered here should provide reasonable bounds on the expected range of the spread parameters for this path and for the conditions of the measurement (i.e., season and phase of the solar cycle). A more comprehensive characterization of the channel requires additional measurements at other locations, during other seasons, and at other periods of the solar cycle.

Manuscript approved March 15, 1995.

[*]In this report, the term auroral oval refers to the region of frequently observed optical aurora as defined by Feldstein and Starkov (1967).

1

2. BACKGROUND

Nominal representations of the geometry of the northern high-latitude region in corrected geomagnetic latitude (CGL) and corrected geomagnetic local time (CGLT) as a function of magnetospheric disturbance index Q have been presented by Whalen (1970) and by Gerson* based on prior work by Feldstein (1966) and Feldstein and Starkov (1967). Geographic features in this representation include the polar cap, the auroral oval, the diffuse auroral region, and the nighttime F layer trough region (Fig. 1). This section briefly describes each of these regions. Hunsucker (1992) provides additional discussions of the region, including an extensive bibliography, in a mini-review paper.

The polar cap is the region of the ionosphere lying poleward of the auroral oval. Under the influence of magnetospherically generated cross-polar electric fields, F layer plasma convects across the polar cap from the noon to the midnight sector and returns via the morning and evening sectors, forming a large scale, two-cell convection pattern (Knudsen 1974; Spiro et al. 1978; Heelis 1982) that extends into and below the auroral oval. The main sources of F region ionization in the polar cap are solar photons, at its sunlit edge, collision-generated ionization caused by electron precipitation within the cap (Weber and Buchau 1981; Buchau et al. 1983), and plasma from lower latitude regions, which is transported into the polar cap by the aforementioned convection process (Buchau et al. 1983; Buchau et al. 1985; Tsunoda 1988). In addition, high-energy solar protons, released during strong solar flares, can enter the polar cap region of the Earth's atmosphere, causing enhanced D layer ionization and associated polar cap absorption and radio "blackout."

The northern auroral oval (Feldstein 1966; Feldstein and Starkov 1967) is asymmetrically distributed about the North Magnetic Pole. The noon sector forms a narrow latitudinal strip centered on a geomagnetic latitude of approximately 75°, while the midnight sector is generally much wider and centered at a lower magnetic latitude (between 65° and 70°). The shape and the latitudinal dispersion of the auroral oval depends on the disturbance index Q. During magnetically disturbed conditions, the oval expands, with the major expansion effects occurring at the nightside, equatorward edge of the oval. Figure 1 shows the geometry for a magnetospheric disturbance index Q = 3, corresponding to magnetically active disturbance conditions. Magnetospheric substorm conditions are usually characterized by disturbance indices in excess of 4.

Auroral region F layer ionization is a combination of photoionization from direct solar illumination, collision-produced ionization from electrons streaming down geomagnetic field lines, and strong plasma blobs that enter the auroral region from the midnight sector of the polar cap (Robinson et al. 1985; Tsunoda 1988). The latter two are the dominant factors in the winter, nighttime auroral ionosphere and give it its unique character.

Familiar effects of enhanced electron precipitation are (1) the visual aurora, (2) increased electron density at D, E, and F layer heights, (3) enhanced auroral radiowave absorption, and (4) enhanced E layer electric currents (the auroral electrojet) and associated geomagnetic field perturbations. The ultimate source of the ionizing electrons is the solar wind. Their entry into the Earth's atmosphere depends on a complicated interaction between the solar wind magnetoplasma

---

*Gerson has prepared a set of polar projection maps of the north polar region with plastic overlays depicting the nominal positions of the auroral oval, F region trough, and diffuse absorption region versus CGLT for several Q values. These are based on the work of Feldstein and Starkov (1967) and of Whalen (1970). Copies of these can be obtained by writing to Dr. Gerson at the following address: Dr. N. Gerson, 9800 Savage Rd., Fort George G. Meade, MD 20755.
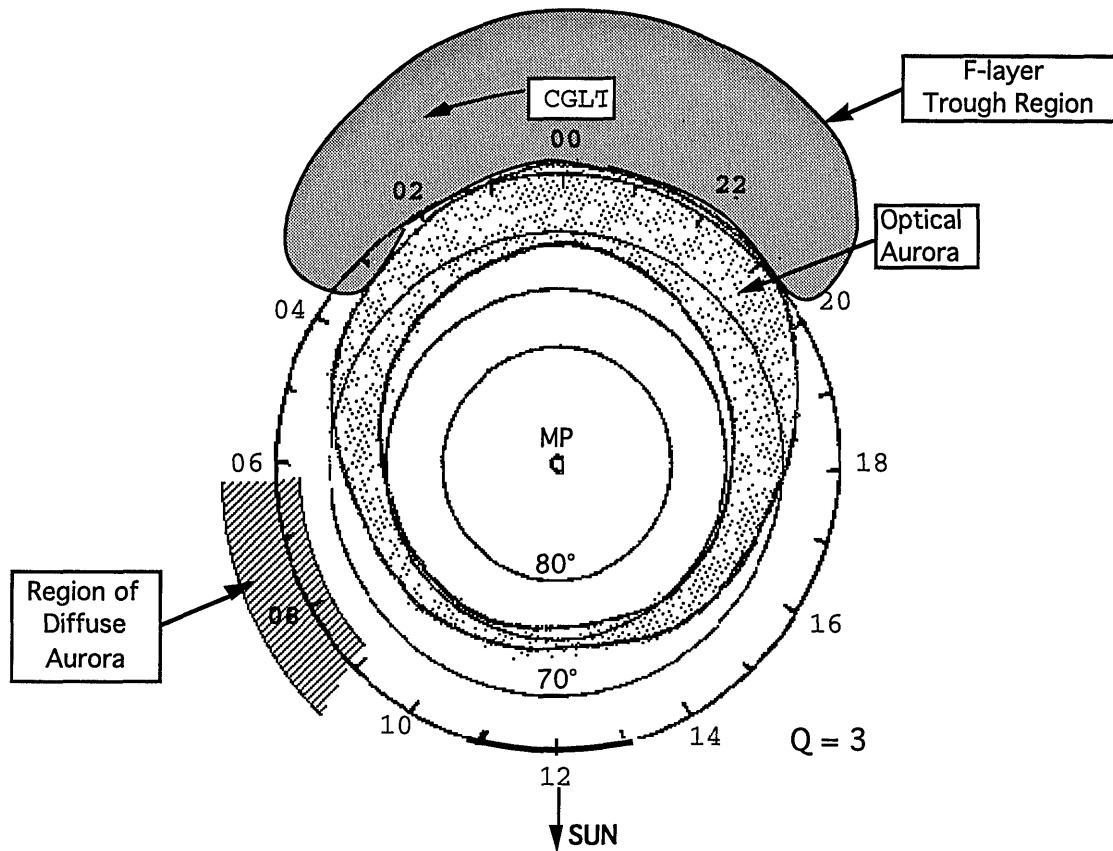
Fig. 1 — Map of the northern high-latitude region in polar projection about
the North Magnetic Pole depicting important features of the region

and the terrestrial magnetosphere. The intensity of this electron precipitation source and of all its manifestations increases with magnetospheric substorm activity. Magnetic activity is a general indicator of substorm activity and, in many cases, is a direct indicator of precipitation activity.

Electron precipitation entering the auroral oval is associated with dayside geomagnetic flux tubes located poleward of the plasmapause that merge with southward pointing field lines of the solar interplanetary magnetic field and become entrained in the two-cell polar convection pattern. The merged field lines are swept across the polar cap and stretched deep into the magnetotail region, where they reconnect with the geomagnetic field from the opposite polar region. The reconnected field lines then "snap back" and merge with the closed field lines of the outer magnetosphere (the plasma sheet) and convect back to the dayside high-latitude region via the dawn and dusk sectors.

Electron energies vary depending on their source region (Whalen 1985). The lowest energy electrons (~0.1 keV) originate within the magnetosheath and represent solar wind particles that gain direct entry to the Earth's atmosphere via geomagnetic field lines that have merged with the interplanetary magnetic field lines of the solar wind. This is the electron energy range that contributes directly to F layer ionization. Electrons of energy in the range 1 to 10 keV originate within the plasma sheet and are responsible for E layer ionization. Energy extracted from magnetospheric field lines during reconnection and "snap-back" is believed to be the energy source

for electrons in the 1 to 10 keV range. Electrons of energy greater than 40 keV are believed to have their source in the high energy trapping region of the closed-field-line magnetosphere (the Van Allen belt). The source of the Van Allen belt electrons is also the solar wind, via the intermediary stage of the plasma sheet. The mechanism for accelerating electrons to and above the 40 keV level is not well understood. Electrons of energy higher than 40 keV are responsible for D layer ionization and associated radiowave absorption.

The deposition height and density of collision produced ionization depends on the energy and the flux of the precipitating electrons. These are highly variable, depending on conditions in the local interplanetary medium and ultimately on conditions on the Sun. This variability, along with that of the direction of the interplanetary magnetic field, gives the auroral ionosphere its unpredictable and rapidly changing character.

Auroral effects are classified as discrete or diffuse based on their temporal and spatial characteristics (Hartz and Brice 1967; Whalen 1985). This includes all observed effects including optical emissions, electron precipitation events, magnetic disturbances, absorption effects, and electron density changes. Discrete auroral effects are observed to occur most frequently at night with a broad maximum centered about 2200 CGLT, while diffuse effects are fairly widespread in magnetic local time but are primarily a morning pheomenon with a broad peak centered on 0800 CGLT (Hartz and Brice 1967). The discrete aurora is generally structured, dynamic, and optically bright, while the diffuse aurora is spatially diffuse, slowly varying, and optically faint. Presumably the discrete aurora is associated with electron precipitation events that are a prompt response to chaotic events in the storm-time solar wind, while the diffuse aurora is related to precipitation events that have been buffered in the closed-field-line ion reservoir of the plasma sheet and dispersed spatially and temporally in the process.

The three energy groups (~0.1 keV, 1 to 10 keV, and >40 keV) are represented in both the discrete and the diffuse aurora but the latitude-time sectors that they affect are different (Whalen 1985). The effects of the low-energy electrons (~0.1 keV) for both the discrete and the diffuse aurora are confined primarily to the auroral oval F layer. For the 1 to 10 keV electrons, which are responsible for E layer effects, the area affected by the discrete aurora is confined to the auroral oval, while that affected by the diffuse aurora overlaps the oval on the nightside but lies just equatorward of the oval on the dayside. In the high-energy domain (>40 keV), the discrete aurora is confined to the nightside oval while the diffuse aurora is found in an annular region between approximately 60° and 66° geomagnetic latitude. The high-energy diffuse aurora overlaps the oval on the nightside but is located approximately 10° below the equatorward-edge of the oval on the dayside. The high-energy diffuse aurora affects primarily the ionospheric D layer and is responsible for enhanced auroral absorption.

The diffuse aurora is present during quiet magnetic conditions as well as disturbed conditions, while the discrete aurora is primarily a disturbance phenomenon. Both are intensified during magnetospheric substorms. During severe substorms, auroral absorption can be strong enough to cause extended periods of radio "blackout," provided the radio propagation path pierces the D layer in regions of enhanced D layer ionization.

The nighttime, midlatitude, ionospheric trough is a region of depressed F layer electron density occupying several degrees of latitude just equatorward of the auroral oval (Muldrew 1965; Sharp 1966; Knudsen 1974; Spiro et al. 1978) and extending from roughly the location of the solar terminator to approximately 2 to 4 hours past the midnight magnetic meridian. Aside from a diminished maximum usable frequency (MUF), the trough region is characterized by a very steep

electron density gradient at its boundary with the auroral oval (Sharp 1966; Spiro et al. 1978). This gradient can be significant in terms of fostering instabilities leading to plasma irregularities and associated radiowave scattering phenomena.

The major factors contributing to the formation of the F layer trough are the opposing effects of (1) the eastward atmospheric corotation with the Earth and (2) the westward polar-cap plasma convection on the evening/nightside of the Earth (Knudsen 1974; Spiro et al. 1978). In a narrow range of latitudes corresponding to the trough, these motions cancel one another with the result that the associated plasma is in darkness for an extended period of time causing a reduction in ionization density by normal recombination processes. The width and depth of the trough has been observed to vary inversely with the intensity of the flux of precipitating electrons of energy less than 80 eV (Sharp 1966). Similarly, it is expected that the width and depth of the trough will show a seasonal dependence because of the strong seasonal variation of the number of daylight hours at high latitudes. Finally, it should be mentioned that the existence of a well-structured, two-cell convection pattern, and as a consequence that of the trough, is dependent upon a southward pointing magnetic field component in the solar wind magnetoplasma (Heelis 1982). Furthermore, the position, size, and depth of the trough are dependent on the magnitude of the cross-polar electric field, which depends on the solar wind speed (Spiro et al. 1978).

The high-latitude ionosphere exhibits a strong seasonal variation because of the effects of changes in solar zenith angle. Similarly, the solar cycle has a major impact on the level of solar ultraviolet radiation that reaches the Earth and on the frequency and intensity of solar flares. It is therefore anticipated that the season and the phase of the solar cycle will have a major impact on the character of the high-latitude ionosphere. The investigation reported here was limited to data acquired during a single season (spring) and year (1988).

3. EXPERIMENT CONDITIONS

The data presented in this report were collected on an 80 km east-west path in the vicinity of Fairbanks, Alaska (Fig. 2) during mid-May of 1988. The geographic coordinates of the midpath point were 64.87° N and 146.83° W. The measurement period came approximately two years after solar minimum of solar cycle 22. It was marked by a solar sunspot index of approximately 85 and by active magnetic conditions, including eight days during the month of May that were affected by strong magnetospheric substorms. Table 1 summarizes the measurement times and applicable geomagnetic conditions. The columns of the table refer to the eight (8) three-hour subdivisions of each universal time (UT) day. The rows represent UT days of the month encompassing the measurement period. Two indices of magnetic activity, K_p and K, are specified in the table. K_p is a planetary index obtained by averaging measured activity indices from a globally distributed group of magnetic observatories, while K is a locally measured index in Alaska. Since substorm activity is a global phenomenon, a planetary index is appropriate to its description. Locally measured K indices, however, frequently correlate better with locally measured disturbance phenomena.

The corrected geomagnetic latitude of the midpath point is 65° N. This path is either subauroral or auroral[*] depending on the time of day and the degree of magnetic activity. During the daytime, the path is subauroral. During late evening to postmidnight hours, the path lies in the nighttime auroral oval or the ionospheric trough region depending on magnetic activity. For a planetary magnetic activity index K_p of three or less, the nighttime path is likely to lie within the trough region.

---

[*]The term auroral is used in this context to indicate a position that lies within the auroral oval (as defined by Feldstein and Starkov (1967)).
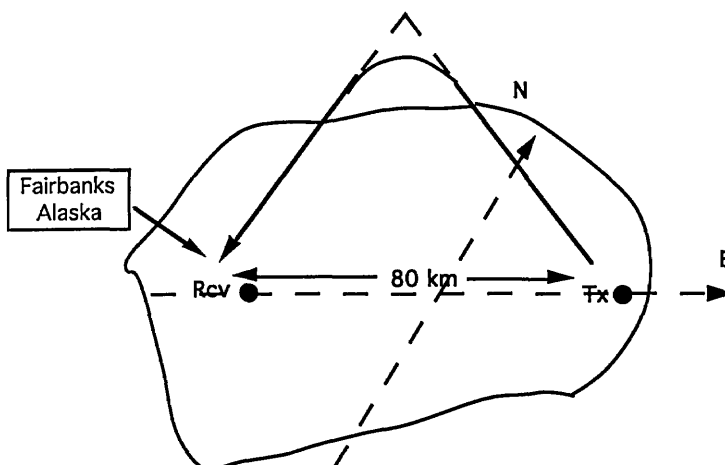
Fig. 2 — Near-vertical incidence measurement path

Table 1 — Calendar of Geomagnetic Activity Levels (K$_p$/K)
and Channel Measurement Periods (shaded areas)

3 Hour Intervals (UT)

MAY	00–03	03–06	06–09	09–12	12–15	15–18	18–21	21–24
1	2/2	1+/1	1+/1	2-/2	1+/1	1+/1	1/1	2-/1
2	1-/2	2-/1	1+/1	2-/2	2/4	2/2	2/2	3/2
3	1+/2	2-/2	2-/2	1/3	1/3	2/1	3-/2	3-/1
4	4-/3	4-/4	2/4	2-/3	3-/3	2/1	4-/2	2/1
5	1+/1	1+/1	3-/3	4+/6	3/6	2-/1	2/2	6/3
6	7-/5	6/6	7+/7	7/6	7/7	7+/6	5+/5	4+/3
7	1+/3	2-/1	2-/2	3/2	3/5	3-/3	3+/3	4/3
8	2+/3	2+/2	2+/2	2+/5	3+/6	4-/5	3/2	3/2
9	2+/2	2-/2	3+/5	3-/5	2+/3	2+/2	2+/3	2/2
10	3+/3	3/3	3/4	2+/4	2/4	2+/3	2-/2	2/2
11	2-/1	2+/2	2+/3	2/4	2-/3	2/2	1/1	1/1
12	3-/2	1/1	1+/1	1/1	1/0	1+/1	1-/1	1+/1
13	2-/1	2-/1	1-/1	1+/3	2-/3	2-/1	1/0	0+/0
14	1-/1	1-/0	1-/1	1/4	1/3	1+/0	1/0	0+/0
15	1+/1	3/4	2-/2	1+/0	1/0	1-/1	1-/0	2-/1
16	2-/2	3-/3	2+/3	3/5	3/4	4-/6	1-/1	2/1
17	2/2	4/5	4-/5	4/5	5/6	4-/3	4-/3	3+/2
18	5/4	3/4	3+/5	3/4	3+/4	2-/3	1+/2	3+/3
19	3-/3	2-/2	2/2	2/3	2-/3	1+/3	1/1	1-/1

1988

For K_p values greater than three, the nighttime path is more likely to lie within the auroral oval because of the equatorward expansion of the oval.

At the latitude of Fairbanks, the spring, daytime ionosphere is dominated by a strong F1 layer and an F2 layer whose critical frequency is not substantially greater than that of the F1 layer. As a result, starting at sunrise and for most of the remainder of the day, F layer returns consist of identifiably distinct F1 and F2 layer returns, with the F2 returns delayed substantially because of retardation in the underlying F1 layer. Furthermore, at most ionospherically supported frequencies, F1 and F2 layer returns are characterized by extensive delay dispersion and correspondingly reduced signal amplitudes. Optimum propagation conditions prevail toward the end of the day when the F1 layer critical frequency declines rapidly, because of its strong dependence on solar zenith angle. At this time of day, the F2 layer is dominant and group delay, delay dispersion, and signal amplitude approach values characteristic of the quiet, daytime, midlatitude channel. These periods of optimum channel conditions can prevail for a period of three to four hours during quiescent ionospheric conditions.

The measurement apparatus used was a multifrequency bistatic HF channel probe that measured the complex pulse response of the HF skywave channel (Wagner and Goldstein 1985; Wagner et al. 1988). The instrument was configured to produce an oblique ionogram record at the beginning of each experiment period followed by an extended interval of probing on a prescribed set of frequencies (usually eight different frequencies). Probing would continue for a period of approximately 14 minutes during which the probing frequency would cycle through the selected set of frequencies. Additional details regarding the operation of the probe are provided in the Appendix.

4. RESULTS

This section is divided into two subsections. Section 4.1 presents general results pertaining to all of the measurements, and Section 4.2 presents detailed results pertaining to selected experiments representative of the range of conditions that may be encountered on the high-latitude channel. For each experiment or group of experiments, a graph showing details of magnetic activity relevant to the measurements is included. The graph includes magnetic activity indices K_p and K and a locally measured magnetogram for a 24-hour period encompassing the measurement interval. Cross-hatched areas on the magnetogram indicate channel probe measurement times. The magnetic fluctuation activity is represented in terms of two distinct time scales, CGLT and UT. CGLT is more useful than UT as a representation of time for describing auroral phenomena. CGLT for Fairbanks lags UT by approximately 11 hours and 15 minutes and lags local meridian time by approximately 1 hour and 15 minutes.

In the discussion of measured results, the location of the path midpoint relative to the auroral oval, the diffuse auroral region, and the F layer trough region is important. As indicated in Section 2, the size and location of these regions is correlated with the intensity of magnetic activity. For a prescribed magnetospheric disturbance index Q, the nominal oval, trough, and diffuse auroral regions can be represented as well-defined regions on a polar projection of the north magnetic polar region.[*] As shown in Fig. 1, the coordinates of this graph are corrected geomagnetic latitude (CGL) and

---

[*]It is important to stress that the size and position of the auroral oval and trough regions, as depicted in these figures, are an average representation based on an extensive observational database. They are not meant to be an actual representation of these features at the time of the measurement. Furthermore, in this report, Q is assigned the value of a measured K_p, or a value intermediate between K_p and K, when K_p and K differ substantially. This may be a dubious assignment, especially for small K_p (Feldstein and Starkov 1967), but is considered acceptable for the qualitative uses made of it in this report.
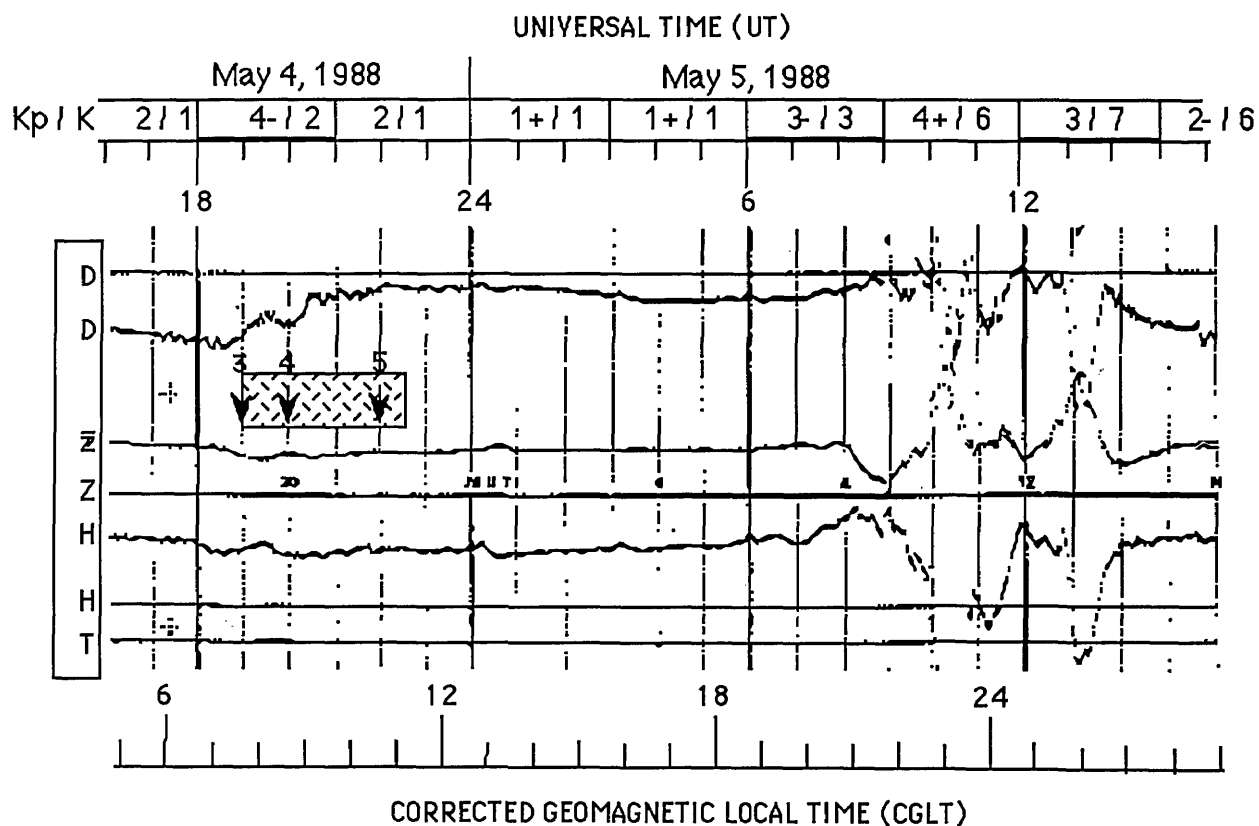
UNIVERSAL TIME (UT)

Fig. 3(a) — Magnetogram and magnetic disturbance indices relevant to Experiments 3, 4, and 5

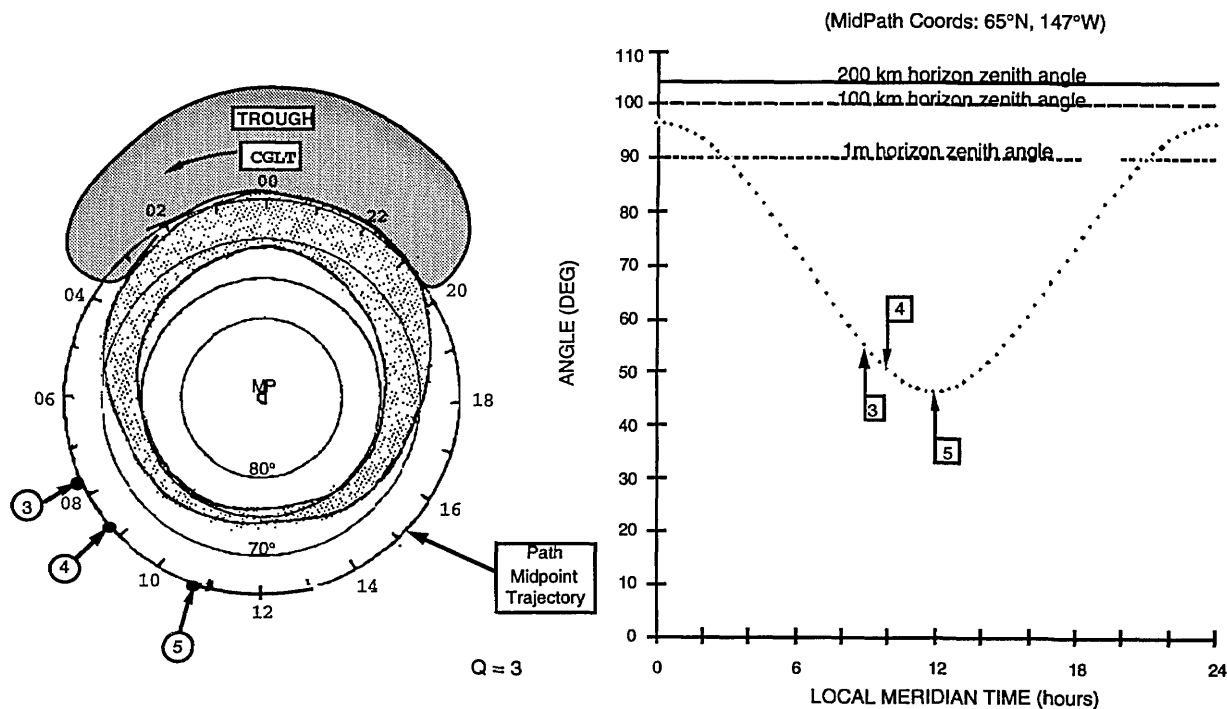Fig. 3(b) — Position of path midpoint relative to oval and trough for Experiments 3, 4, and 5 and for disturbance index Q = 3

Fig. 3(c) — Solar zenith angles for Experiments 3 to 5

CGLT. In this representation, the position of the path midpoint vs CGLT is a circle (CGL = 65°) centered on the geomagnetic pole and its position relative to all auroral features can be readily determined given values for Q and time. A diagram of this type is included for each experiment group, with markers representing the path midpoints for individual experiments.

As mentioned in Section 2, the diffuse auroral absorption region is confined to a magnetic latitude interval between 60° and 66°, while the magnetic latitude of the path midpoint is at 65°. It is, therefore, clear that enhanced radiowave absorption may be anticipated at times of enhanced magnetic activity when enhanced 40 keV diffuse electron precipitation is likely.

An additional factor affecting the state of ionization in the ionosphere is the solar zenith angle (SZA) vs local meridian time (LMT). In each discussion of a single experiment or group of experiments, a curve showing the SZA at the measurement time(s) is included. In all cases, the SZA is evaluated for the Fairbanks location and for a solar declination corresponding to mid-May 1988. In addition to showing the variation of SZA with LMT, the curve also indicates the horizon zenith angle as measured from altitudes of 1 m, 100 km, and 200 km.

4.1 General Results

This section briefly describes each measurement group shown in Table 1. It includes general comments that summarize the measurement conditions and the results.

4.1.1 Measurements of May 4, 1988, 1900 to 2215 UT (Experiments 3, 4, and 5)

These were morning measurements (0900 to 1215 LMT, 0745 to 1100 CGLT) during a period of relatively quiet magnetic conditions. The local K index varied between a value of 2 at the start of the measurement series to a value of 1 at the end. Surprisingly, K_p was substantially larger than K with values of 4- at the start and 2 at the end of the measurement series. The probe was configured for fine delay resolution (wide signal bandwidth) and a narrow Doppler window based upon what were expected to be benign propagation conditions.

Figure 3(a) shows a local magnetogram made at the College Magnetic Observatory for May 4 - 5. The cross-hatched rectangle indicates the period of channel probe measurements, with arrows indicating experiment start times. Note that the time scale above the magnetogram is UT while that below is CGLT. The magnetogram shows a minor fluctuation of the horizontal (H) and vertical (Z) components of the geomagnetic field and a somewhat larger fluctuation of the magnetic deviation (D) during the measurement series. These may be compared with the storm time fluctuations observed between 0800 and 1500 UT of May 5 on the same figure. During the storm, K_p varied between values of 4+ and 2 while the locally measured K index fluctuated between values of 6 and 7. The position of the propagation path relative to the auroral oval (stippled region) and the trough (shaded region) is drawn in Fig. 3(b) for an assumed magnetospheric disturbance index of Q = 3. Because of the discrepancy between the measured values of K_p and K (4- and 2, respectively), a compromise value of Q = 3 was selected as representative of magnetospheric activity for this event. Figure 3(b) indicates that the propagation path was quite distant from the auroral oval and trough regions and should not have been affected by an auroral disturbance except possibly for an auroral absorption event. Based on the conditions described in Figs. 3(a) and 3(b), and those of Fig. 3(c), which describes the relevant solar zenith angles for the experiments, one would expect a normal

morning buildup of the E and F1 layers of the ionosphere, with little disruption due to auroral effects except possibly for some weak absorption. It should be noted that these conclusions would not have been significantly affected if Q values of 4 or 2 were used for drawing the auroral oval in Fig. 3(b).

Signals were observed to be weak during this entire set of measurements but there was no evidence of scattered signals. F layer channel scattering functions indicated delay-spreads as large as 300 μs near the layer critical frequencies, but negligible Doppler-spreading of signals. The ionograms showed evidence of weak, but otherwise normal 1E, 1F1, and 1F2 traces (e.g., Fig. 4). The low signal-to-noise ratio (SNR) is attributed to a combination of factors including the wide signal bandwidth, a high noise and interference background, and the extensive delay dispersion inherent in an ionosphere in which E, F1, and F2 layers have critical frequencies that span an interval of just 2 MHz. A gradual weakening of the ionogram traces in the time between Experiments 3 and 5 and an increase in the lowest observable frequency suggest that a minor diffuse absorption event may have been in progress over that time period.
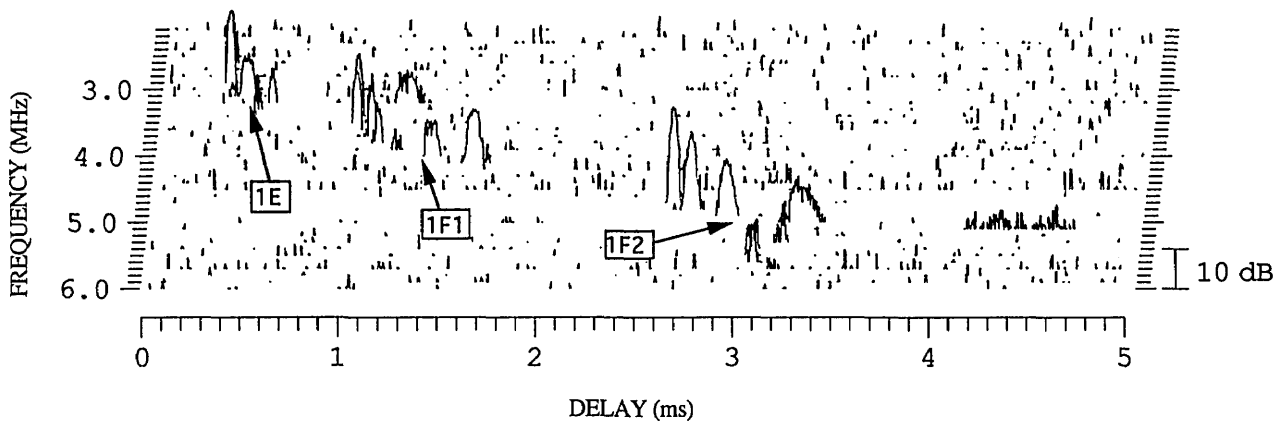
Fig. 4 — Morning ionogram, Experiment 3, May 4, 1988, 1900 UT, delay origin = 0.5 ms

4.1.2 Measurements of May 6, 1988, 0030 to 0300 UT (Experiments 6, 7, and 8)

These were afternoon measurements (1430 to 1700 LMT, 1315 to 1545 CGLT). Magnetic, geometric, and solar conditions relevant to the propagation path are shown in Figs. 5(a-c). The measurements coincided with the onset of a "great" magnetic storm as can be seen from the magnetogram of Fig. 5(a). The K-indices for the measurement period had values of 7- for K_p and 5 for K, and were preceded by a three hour period of unsettled magnetic conditions as indicated in Fig. 5(a). A value of Q = 6 was assumed for the magnetospheric disturbance index Q for the period of interest. The auroral geometry, Fig. 5(b), indicates that the path midpoints lie below the auroral oval and trough regions but within the diffuse auroral absorption zone (CGL between 60° and 66°). Solar zenith angles for the measurement period, Fig. 5(c), indicate afternoon conditions.

The start of the measurement series coincided with a large peak in the H component of the magnetic field perturbation, which probably constituted the sudden commencement phase of the ensuing magnetic storm. An ionogram (not shown here) made at 2330 UT (1215 CGLT), shortly before the storm sudden commencement, showed clear evidence of normal E and F1 layer traces and a weak F2 layer trace. E layer returns were observable down to a minimum frequency of ≈2.3 MHz.
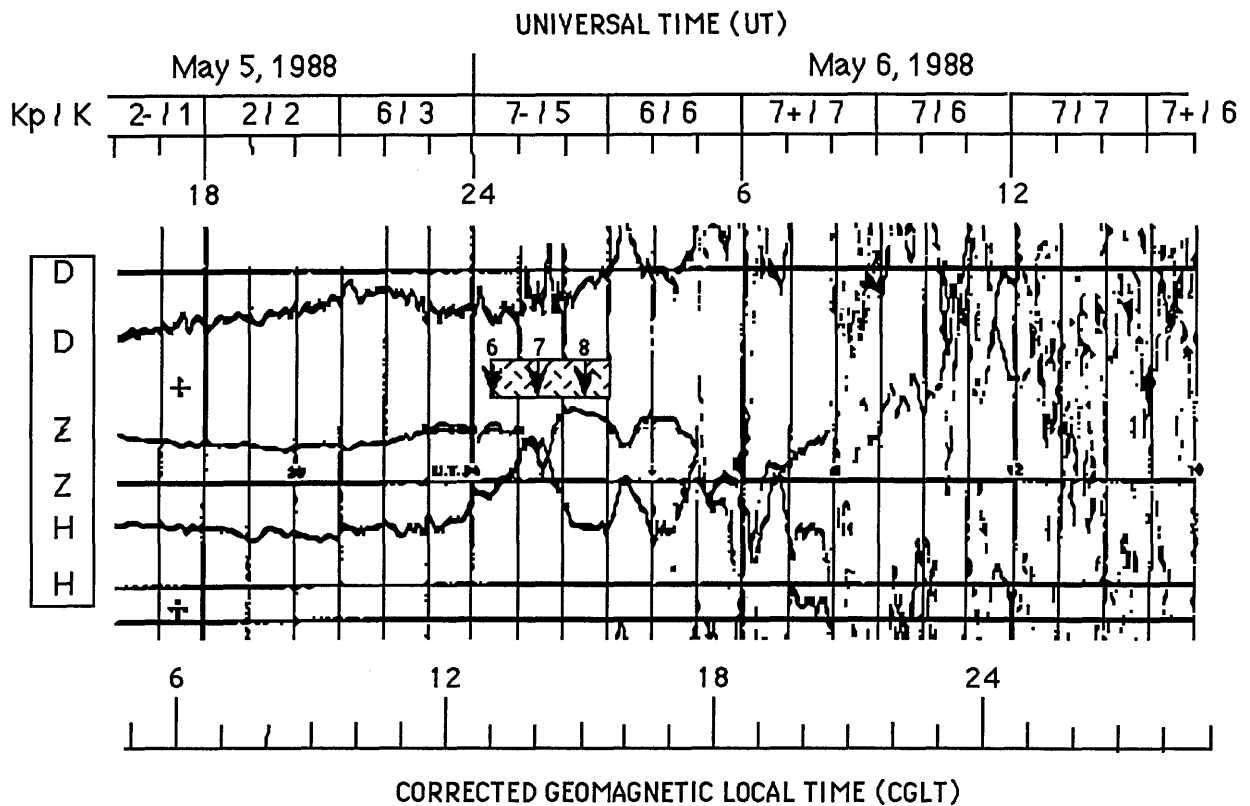
UNIVERSAL TIME (UT)

Fig. 5(a) — Magnetogram and magnetic disturbance indices relevant to Experiments 6 to 8

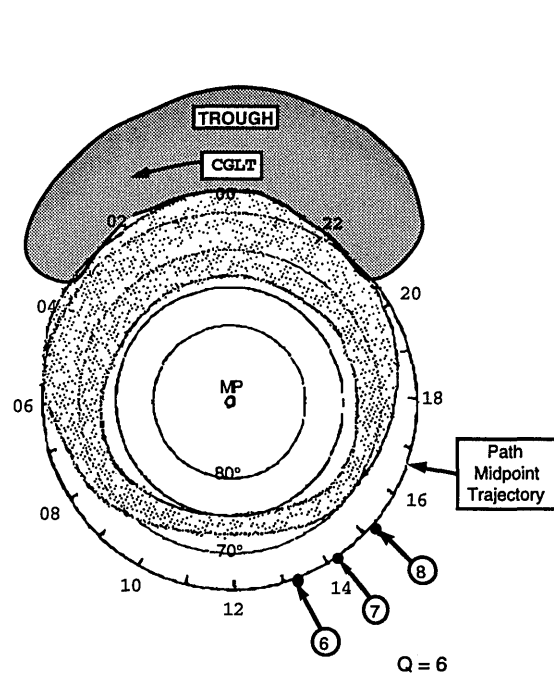
Fig. 5(b) — Position of path midpoint relative to oval and trough for Experiments 6 to 8 and for disturbance index Q = 6
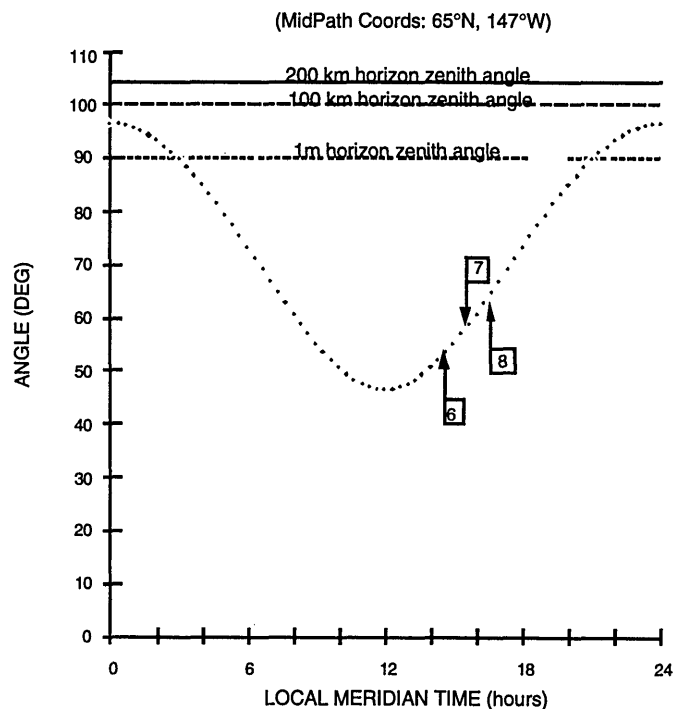

Fig. 5(c) — Solar zenith angles for Experiments 6 to 8

Experiment 6 was conducted during the latter part of the buildup phase of the storm sudden commencement. An ionogram made during Experiment 6 (not shown here) showed no returns below 5 MHz and weak F2 layer returns at and above 5 MHz. This indicated a sharp increase in absorption levels coinciding with the magnetic perturbation and presumably associated with high energy electrons of the diffuse aurora. Scattering functions for the observed F2 layer returns indicated Doppler-spreads of less than 1 Hz.

Experiment 7 was in progress at the peak and during the decay phase of the magnetic perturbation associated with the storm sudden commencement. The ionogram for Experiment 7 (Fig. 6) showed the presence of weak sporadic E (E$_s$) between 2.5 and 4 MHz and a weak, substantially delayed 1F2 return at frequencies above 4.5 MHz. Evidence of a partial recovery from the effects of the absorption event came later in the experiment in the form of a gradual emergence of a strong but extensively dispersed 1F1 return.

Experiment 8 was conducted during a short-lived period of reduced magnetic activity following the storm sudden commencement. The ionogram (not shown here) shows a well-defined but very weak E layer return from either the normal E layer or a thick, refracting sporadic E layer. The O-mode critical frequency of the E layer return was approximately 3.2 MHz while the X-mode critical frequency appeared to be about 3.9 MHz. F layer returns were too weak to be useful for analysis.

These experiments show the strong association between magnetic storms and enhanced absorption for this path. There also appears to be some evidence for weak, storm-associated sporadic E and for a modest increase in Doppler-spread.
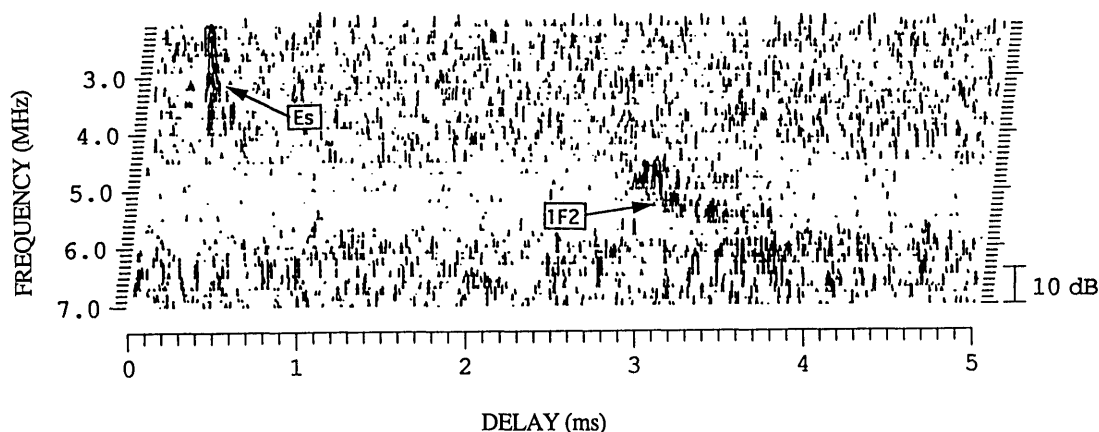

Fig. 6 — Afternoon ionogram, Experiment 7, May 6, 1988, 0130 UT, delay origin = 0.5 ms

4.1.3 Measurements of May 7, 1988, 1400 to 2015 UT (Experiments 9 to 15)

These were postmidnight to early morning measurements (0400 to 1015 LMT; 0245 to 0900 CGLT). They were made over a period during which K$_p$ varied between values of 3- to 3+ and K diminished rapidly from an initial value of 5 to a final value of 3. The local magnetogram for this period is shown in Fig. 7(a). The first experiment (No. 9) occurred shortly after a large negative perturbation of the H component of the magnetic field. The remaining experiments in this group were conducted during a period of active magnetic conditions, as is evident from the small, but persistent, fluctuations of all traces on the magnetogram.

UNIVERSAL TIME (UT)

May 7, 1988

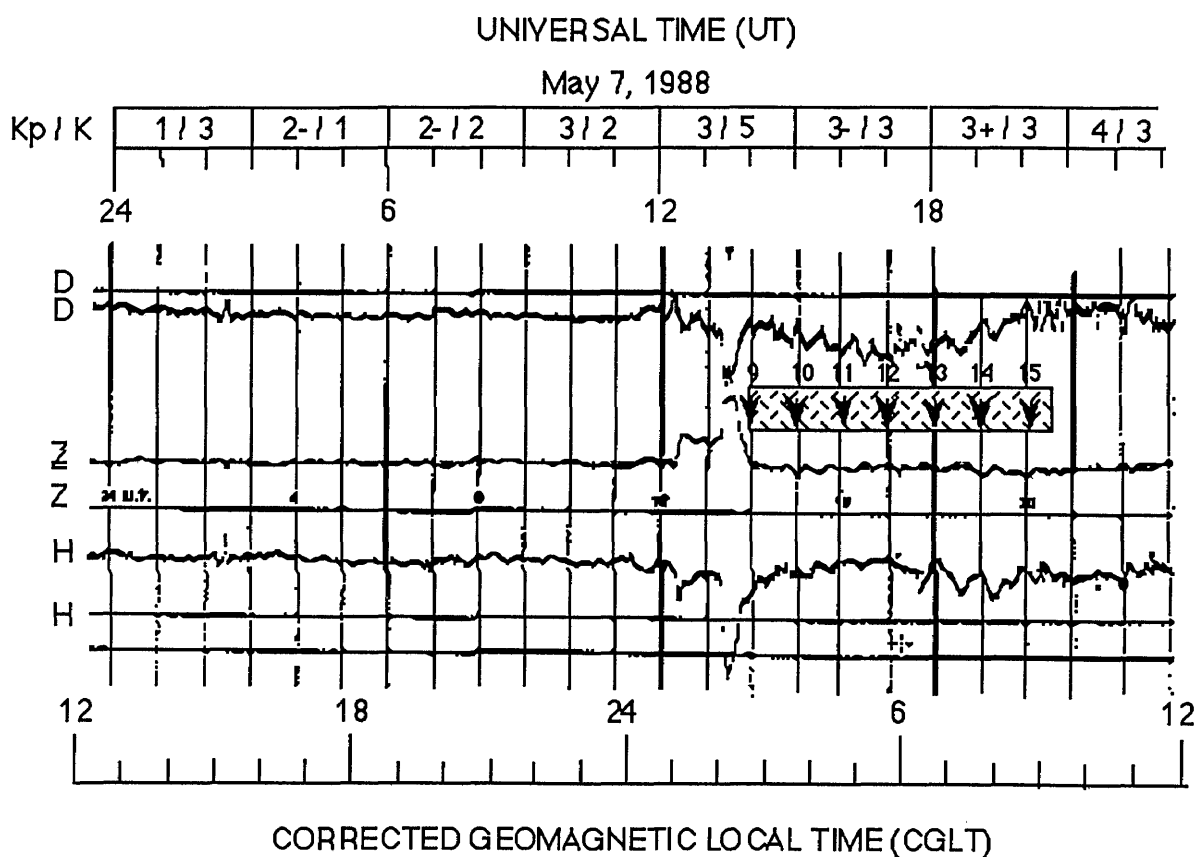

CORRECTED GEOMAGNETIC LOCAL TIME (CGLT)

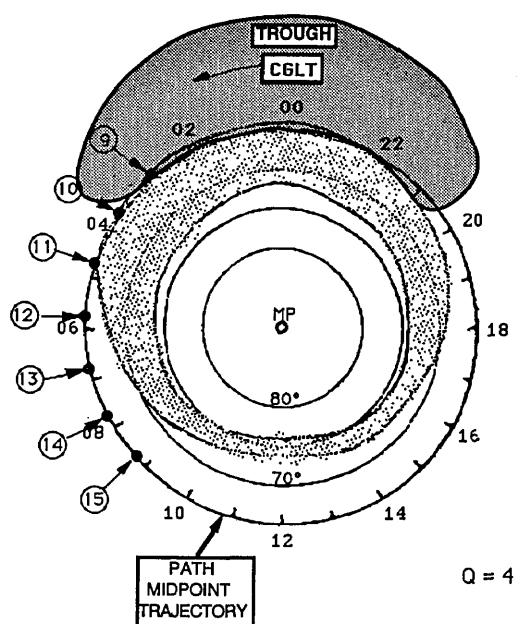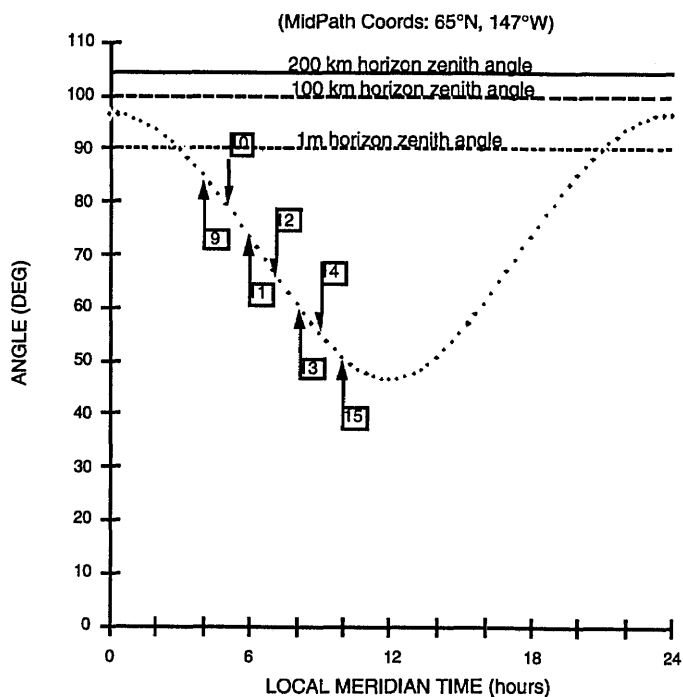Fig. 7(a) — Magnetogram and magnetic disturbance indices relevant to Experiments 9 to 15

Fig. 7(b) — Position of path midpoint relative to oval and trough for Experiments 9 to 15 and for disturbance index Q = 4

Fig. 7(c) — Solar zenith angles for Experiments 9 to 15

This page intentionally left blank.

The location of the path midpoint relative to the auroral oval and trough regions, for all experiments in this group, is shown in Fig. 7(b) for a Q value of 4. Based on Fig. 7(b), Experiment 9 is located at the border between the oval and the trough regions, while Experiments 10 and 11 are located beyond the trough region but at the equatorward edge of the oval. Experiments 12 to 15 are all subauroral but within the latitude interval that is subject to the effects of the diffuse aurora.

The solar zenith angle diagram of Fig. 7(c) shows that the SZA was greater than 70° for Experiments 9, 10, and 11, and decreased to a morning value of 50° by 1000 LMT (Experiment 15). The minimum SZA for this date was 45° at local noon.

Ionograms for Experiment 9 (not shown here) show only a weak sporadic E return, visible over a restricted range of frequencies (2.4 to 2.7 MHz at the start and 3.5 to 4.2 MHz at the end of Experiment 9). The absence of any other returns indicates that an absorption event was in progress. It is unclear whether the absorption event was associated with the discrete aurora or the diffuse aurora but the impulsive nature of the initial magnetic perturbation would suggest the discrete aurora. The visibility of a fragmentary E_S return may indicate that the absorption was not so large as to totally obscure the strongest E_S returns. In Experiment 10, conducted one hour later, conditions had changed and the ionogram (Fig. 8) shows a strong, double-layered sporadic E return, implying that the absorption event had subsided. No other returns were visible out to the highest probe frequency (5.5 MHz), suggesting that they were most likely blanketed by the sporadic E layer.

In subsequent experiments (11 to 13) corresponding to times 0445 to 0645 CGLT (0600 to 0800 LMT), direct solar effects began to exert an influence. The sporadic E layer gradually disappeared and strong, well-defined E, F1, and F2 traces began to appear on the ionograms. In Experiment 13, the ionogram traces weakened and showed evidence of weak multipath. Conditions worsened thereafter and heavy absorption caused total radio blackout during Experiments 14 and 15 (0745 to 0915 CGLT). The resumption of strong auroral absorption appears to be associated with the occurrence of enhanced fluctuations on all components of the magnetogram between 0630 and 0900 CGLT. These fluctuations occurred at a time when effects of the diffuse aurora tend to be most pronounced. The resurgent absorption is assumed to be evidence of the presence of high energy (>40 keV) electron showers associated with the diffuse aurora. The presence of enhanced 1 to 10 keV electron precipitation within the auroral oval could be the cause of the enhanced magnetic fluctuations observed at this subauroral location during this period.
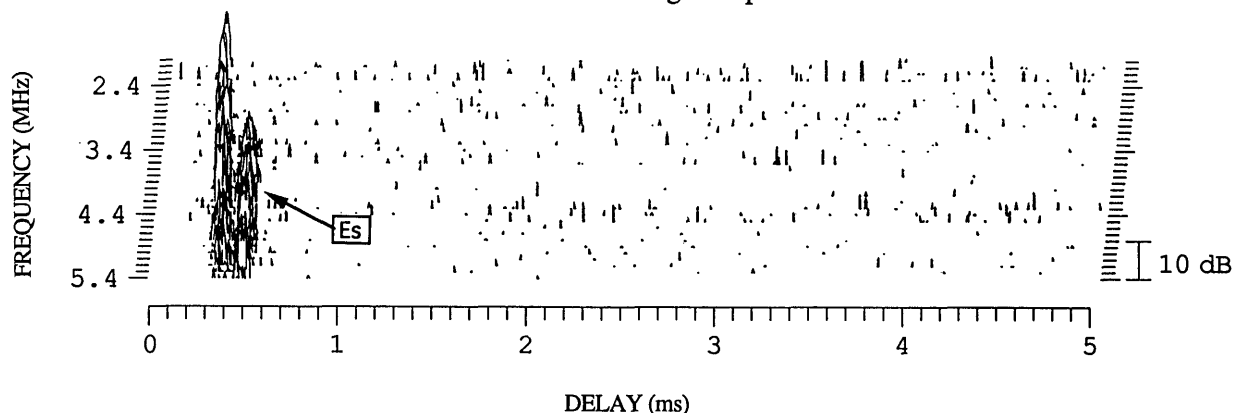

Fig. 8 — Postmidnight ionogram, Experiment 10, May 7, 1988, 1500 UT, delay origin = 0.5 ms

UNIVERSAL TIME (UT)
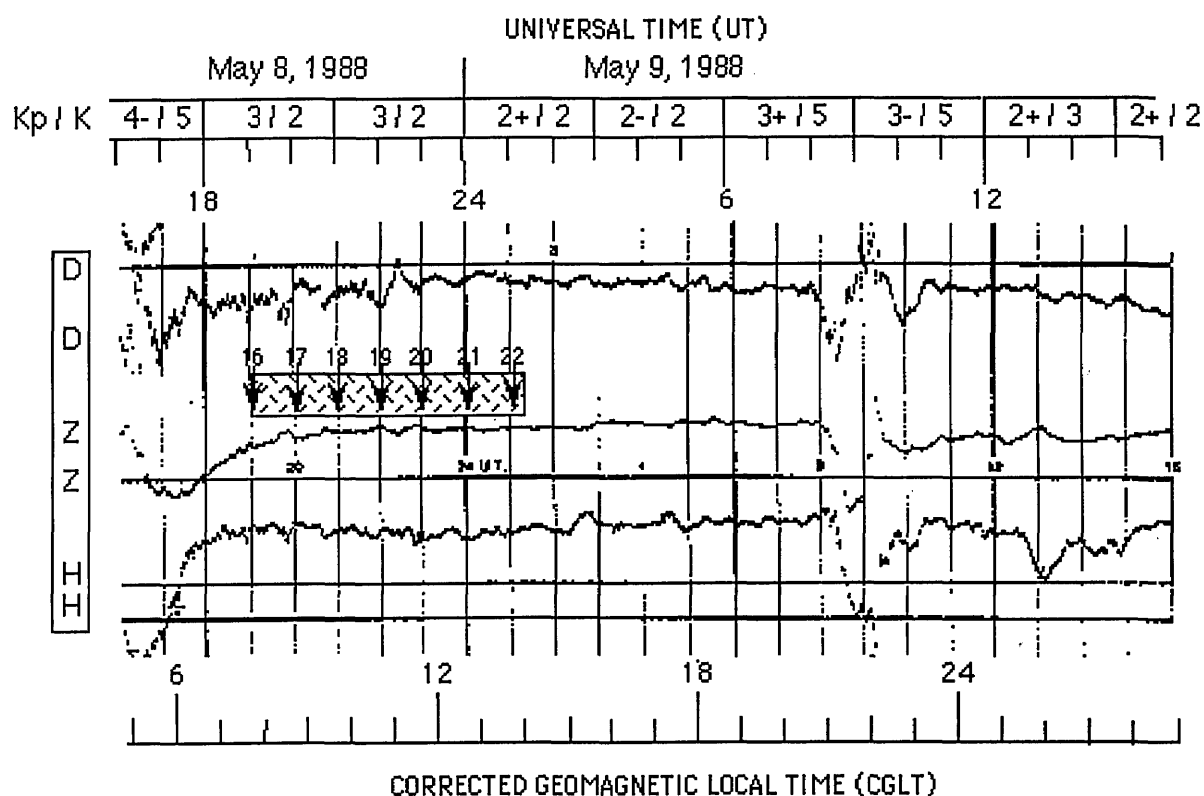
May 8, 1988 | May 9, 1988

Fig. 9(a) — Magnetogram and magnetic disturbance indices relevant to Experiments 16 to 22
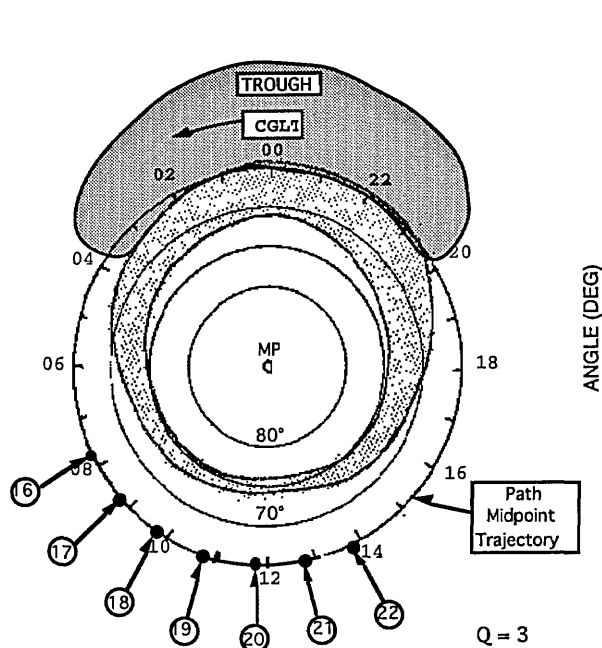
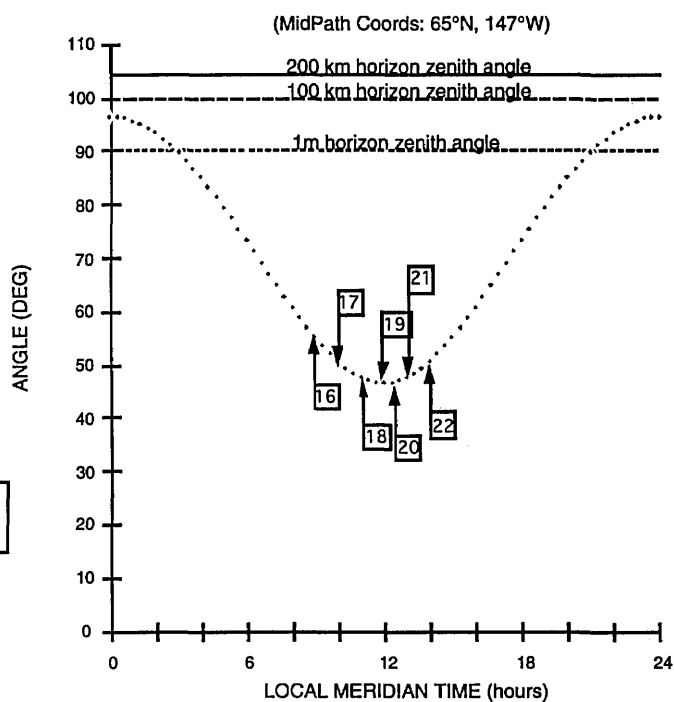Fig. 9(b) — Position of path midpoint relative to oval and trough for Experiments 16 to 22 and for disturbance index $Q = 3$

Fig. 9(c) — Solar zenith angles for Experiments 16 to 22

4.1.4 Measurements of May 8-9, 1988, 1915 to 0115 UT (Experiments 16 to 22)

This set of measurements was conducted during a six hour period around local noon (0900 to 1515 LMT; 0745 to 1400 CGLT) at a time of "unsettled" magnetic conditions. The measurement period followed a magnetic storm during which K_p attained a maximum value of 4- while the local K index peaked at a value of 5. Values for K_p and K during the measurement period were 3 and 2, respectively. A magnetogram illustrating magnetic conditions during the measurement period is shown in Fig. 9(a). The position of the midpath point(s) relative to the auroral oval and the F layer trough region is illustrated in Fig. 9(b), which indicates that all measurements were conducted at subauroral locations. Figure 9(c) shows the SZA at the start of each experiment and indicates that solar photon effects should be at their peak.

Despite the relatively subdued magnetic activity following the magnetic storm, probe signals were either weak or undetectable during the entire measurement period. When ionogram traces were visible, as in Experiment 19, the traces were observed to be normal but weak (Fig. 10). Other ionograms in this measurement series (not included in this report) indicate that periods of enhanced signal absorption alternated with periods of lesser absorption. For example, no probe signals were detected in Experiment 16, while E and F1 layer returns were visible in Experiment 17. The E layer return was substantially weaker than the F1 layer return, however, implying that absorption, while considerably diminished from its earlier levels, was still a factor. The traces continued to strengthen through the early ionogram of Experiment 19 (Fig. 10). In the final ionogram of Experiment 19, the E layer return weakened substantially compared with that of the F1 and F2 returns, indicating the resurgence of an absorption effect. Experiment 20 showed only a barely detectable F2 layer return indicating almost total radio blackout, while Experiments 21 and 22 showed clearly discernible but very weak evidence of F layer returns.

Magnetic activity and diffuse electron precipitation events are known to be correlated with the global ring current that accompanies a magnetic storm. At subauroral latitudes, storm-time magnetic fluctuations result primarily from fluctuations in the global ring current. During the recovery phase of a magnetic storm, the ring current is known to be chaotic, which might explain the observed small, rapid fluctuations of the magnetic field.

Diffuse electron precipitation events (>40 keV), while contributing strongly to enhanced absorption at the latitude of the midpath points for this experiment group, should have little effect on overhead E layer conductivity and associated local magnetic effects.
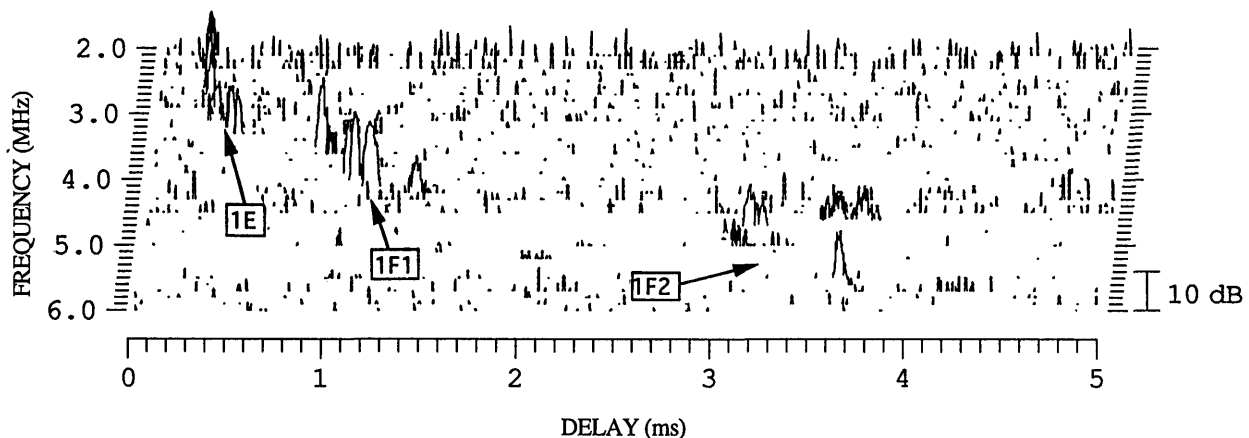

Fig. 10 — Pre-noon ionogram, Experiment 19, May 8, 1988, 2200 UT, delay origin = 0.5 ms
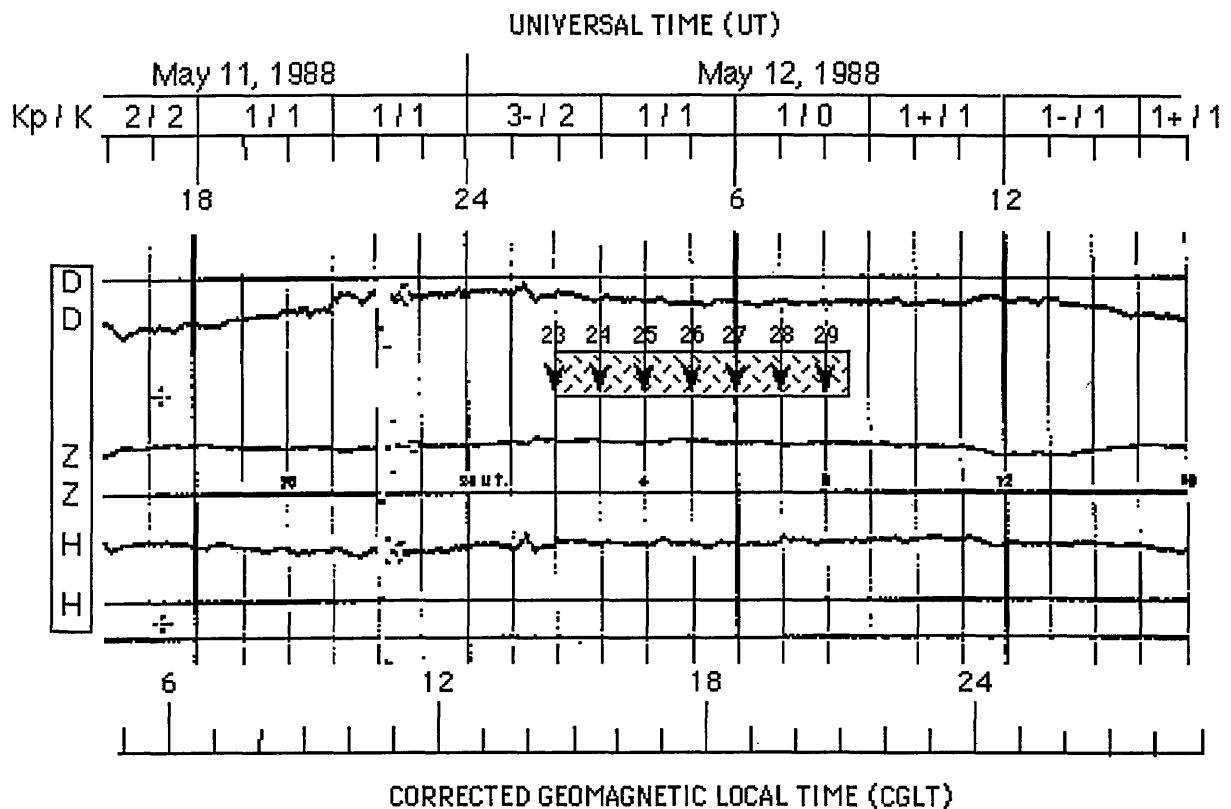
UNIVERSAL TIME (UT)

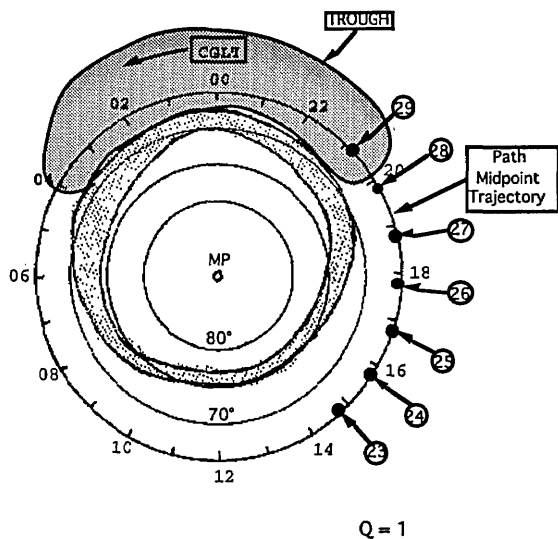Fig. 11(a) — Magnetogram and magnetic disturbance indices relevant to Experiments 23 to 29

Fig. 11(b) — Position of path midpoint relative to oval and trough for Experiments 23 to 29 and for disturbance index Q = 1
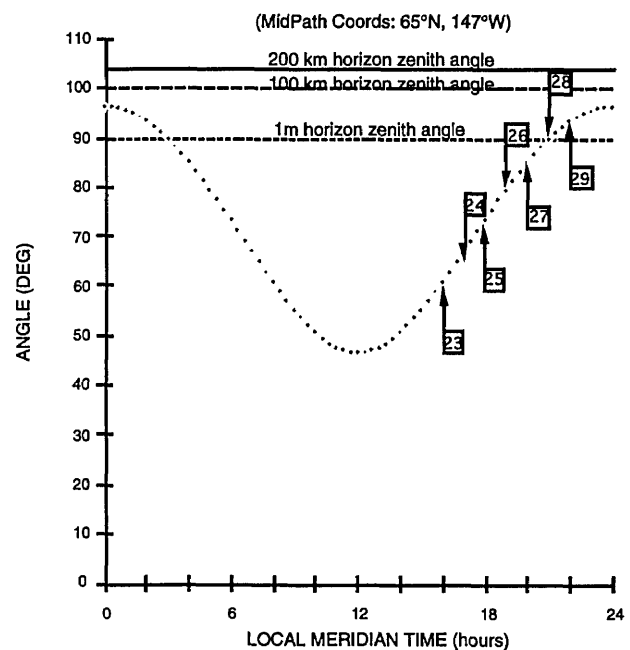
Fig. 11(c) — Solar zenith angles for Experiments 23 to 29

4.1.5 Measurements of May 12, 1988, 0200 to 0830 UT (Experiments 23 to 29)

These measurements were made during the late afternoon to evening hours (1600 to 2230 LMT, 1445 to 2115 CGLT). Magnetic activity was negligible except for a minor fluctuation that occurred approximately 45 minutes prior to the start of Experiment 23. The fluctuation raised the local K index to 2 for that 3-h interval. The fluctuation may have been larger at other observing stations because the K_p value for this measurement interval was 3-. During the remainder of the measurement period, both K indices remained at values of 1. A magnetogram describing magnetic activity during this experiment series is shown in Fig. 11(a).

The location of the path midpoint(s) relative to the auroral oval and trough regions is shown in Fig. 11(b) for an assumed Q value of 1. It can be seen from this figure that the paths are all subauroral and outside the trough region except for that of Experiment 29, which lies within the early part of the nominal trough region. The midpath point for Experiment 29 is on the order of 500 km from the oval-trough boundary, the region most susceptible to irregularity generation.

The solar zenith angles corresponding to this set of experiments is presented in Fig. 11(c). The period of observation is seen to encompass early afternoon times, when direct solar photo-ionization is a dominant factor in ion production, to dusk, when other factors begin to predominate. The early experiments of this group should be characterized by strong F1 layer effects, which gradually diminish as the SZA increases.

Ionograms for this period show normal traces. A prominent F1 layer was observed during the first of these experiments (23) but weakened rapidly in succeeding experiments. The slope of the ionogram trace was observed to decrease over the measurement interval with a corresponding reduction in delay dispersion. Optimal signal transmission conditions prevailed during Experiments 26, 27, and 28 (1900 to 2200 LMT, 1745 to 2045 CGLT) when retardation of the F2 layer due to the underlying F1 layer was no longer a factor. Figure 12 is an ionogram (Experiment 27) illustrating these optimal conditions. The measurement path of Experiment 29 lay within the nominal trough region, as indicated on Fig. 11(b). The path midpoint was well removed from the oval-trough boundary, however, and the received signal showed no evidence of enhanced delay-spread or Doppler-spread.

Spread parameters for this experiment series were found to be among the smallest observed and are representative of magnetically quiet daytime conditions. Section 4.2.1 provides further discussion of the spread parameters for Experiment 27.
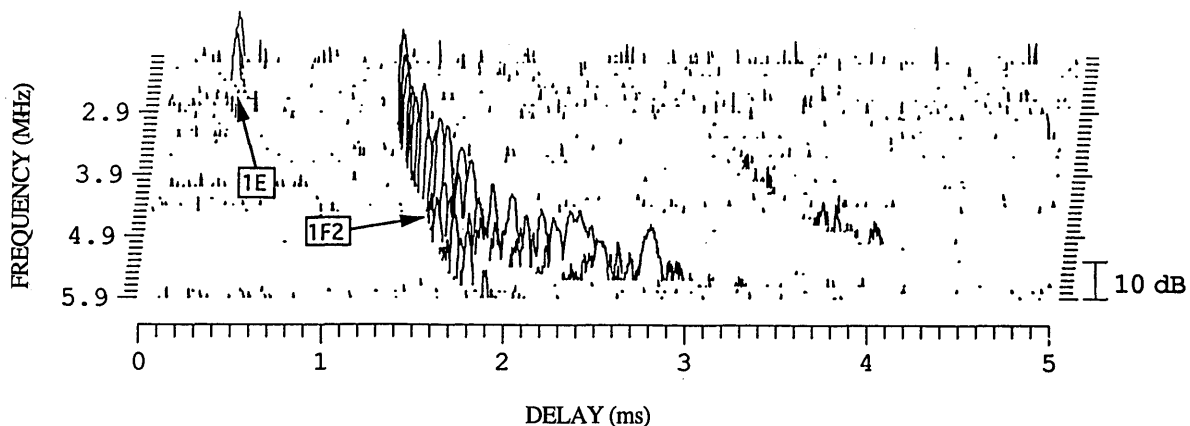

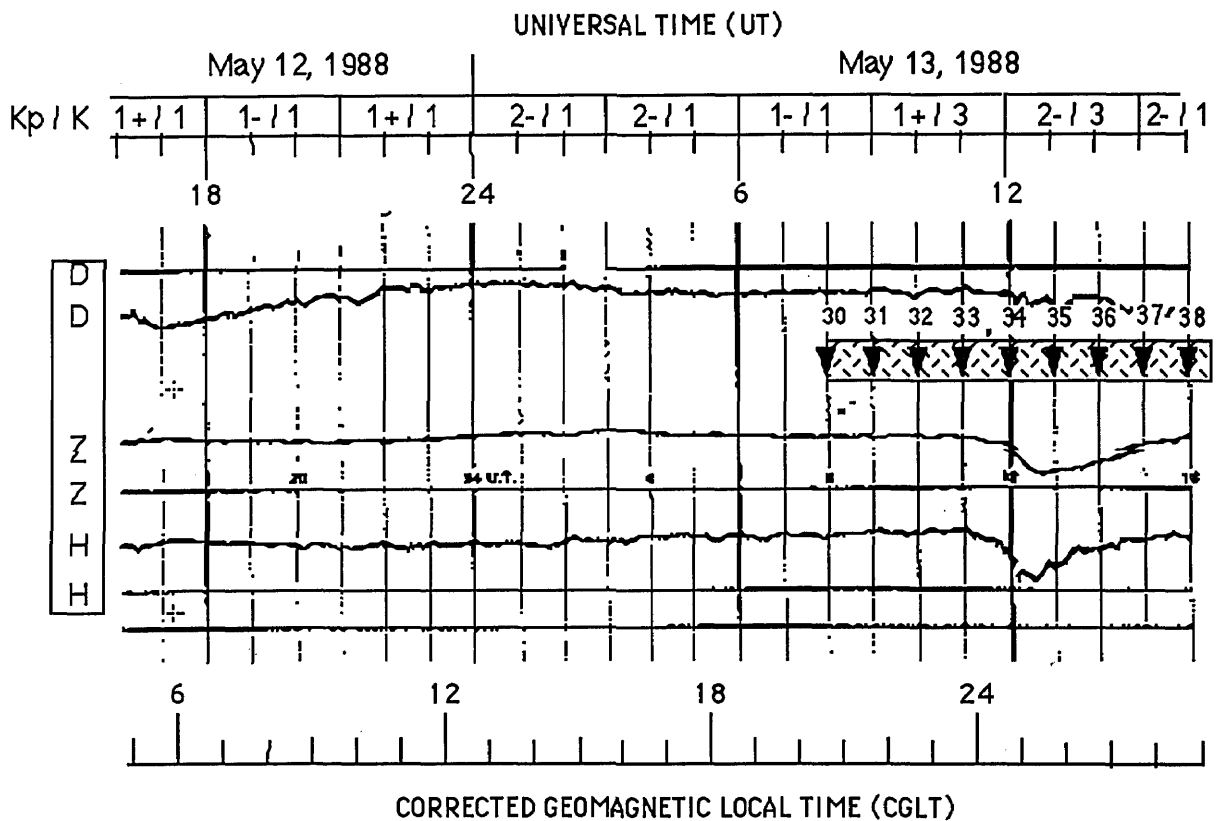Fig. 12 — Late aftenoon ionogram, Experiment 27, May 12, 1988, 0600 UT, delay origin = 0.5 ms

UNIVERSAL TIME (UT)

May 12, 1988 | May 13, 1988

Kp / K | 1+ / 1 | 1- / 1 | 1+ / 1 | 2- / 1 | 2- / 1 | 1- / 1 | 1+ / 3 | 2- / 3 | 2- / 1 |

18   24   6   12

D
D
Z
Z
H
H

30 31 32 33 34 35 36 37 38

6   12   18   24

CORRECTED GEOMAGNETIC LOCAL TIME (CGLT)

Fig. 13(a) — Magnetogram and magnetic disturbance indices relevant to Experiments 30 to 38

TROUGH

CGLT

MP

80°

70°

Path
Midpoint
Trajectory

Q = 2

(MidPath Coords: 65°N, 147°W)

200 km horizon zenith angle

100 km horizon zenith angle

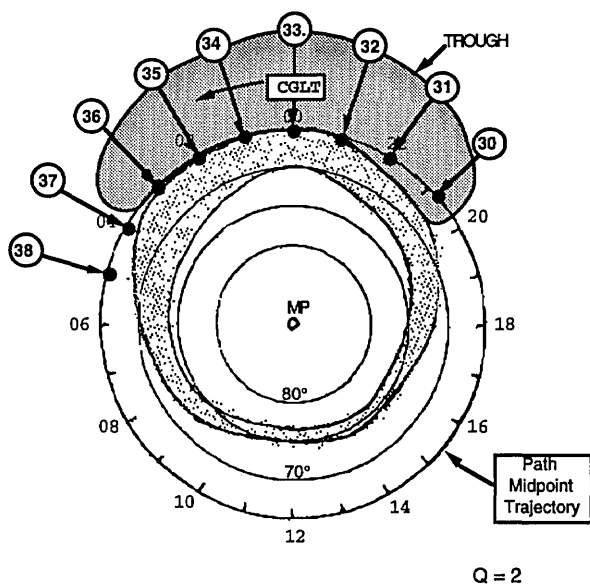1m horizon zenith angle

ANGLE (DEG)

LOCAL MERIDIAN TIME (hours)

Fig. 13(b) — Position of path midpoint relative to oval and trough for Experiments 30 to 38 and for disturbance index Q = 2
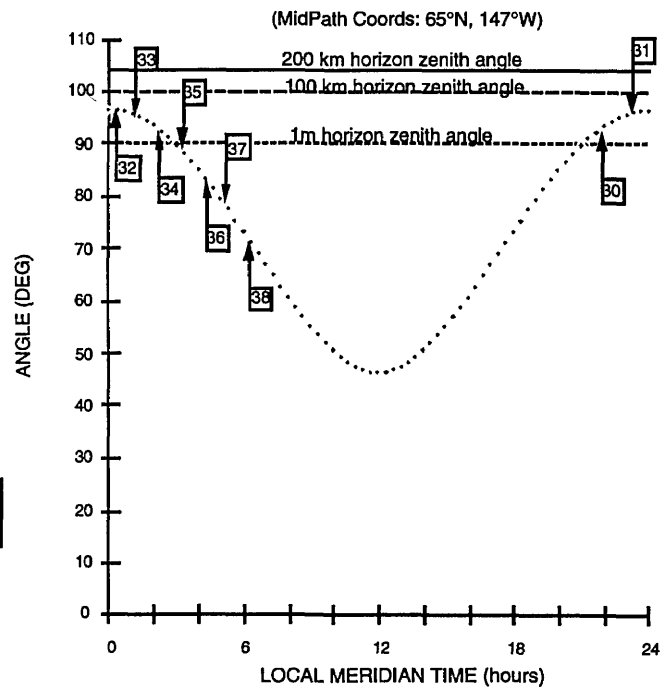
Fig. 13(c) — Solar zenith angle for Experiments 30 to 38

4.1.6 Measurements of May 13, 1988, 0800 to 1630 UT (Experiments 30 to 38)

These were late evening to early morning measurements (2200 to 0630 LMT, 2045 to 0515 CGLT). Magnetic conditions were quiet during this period except for a large, isolated magnetic fluctuation that occurred between the hours of 1100 and 1400 UT. This had only a modest effect on the K_p index, which varied between values of 2- and 1, but had a more marked effect on the local K index, which varied between values of 3 and 1. A magnetogram summarizing conditions during this experiment is shown in Fig. 13(a). The magnetogram indicates that magnetic conditions were quiet during Experiments 30 to 33. A time plot of the position of the midpath point relative to the oval and the trough regions, for an assumed Q of 2 (Fig. 13(b)), indicates that trough or oval effects might be anticipated in the data. An ionogram (not shown here) made during the first experiment of this group (30) shows a weak but otherwise normal-looking F layer trace. The lowest frequencies are the weakest, suggesting a mild absorption event. Frequencies near the F layer critical frequency are weak and diffuse, suggesting the presence of ionospheric irregularities in the vicinity of the F layer peak, which may be a precursor of range-spread ionograms observed in subsequent experiments.

From Fig. 13(b), it can be seen that the position of the path midpoint was approaching the oval-trough boundary during Experiment 31 and lay on the boundary during Experiments 32 and 33. The ionogram for Experiment 31 (Fig. 14(a)) indicates a strong but somewhat irregular F layer trace that becomes weaker and more diffuse as the frequency approaches the F layer critical frequency. During Experiment 33 (Fig. 14(b)) the ionogram trace develops into a range-spread spread F trace. It is worth noting the presence of a second trace in Fig. 14(a), delayed on the order of 500 μs from the main return. This return is presumed to be the result of side-reflection/scatter from an off-path irregularity region. Based on its relative delay, it is estimated that the irregularity region is laterally displaced from the propagation path by ~230 km. Assuming that the region lies to the north of the baseline, that would place it at the oval-trough boundary or slightly within the oval. Section 4.2.2 discusses details of the channel spread characteristics for Experiments 31 and 33, representative of quiet nighttime conditions.
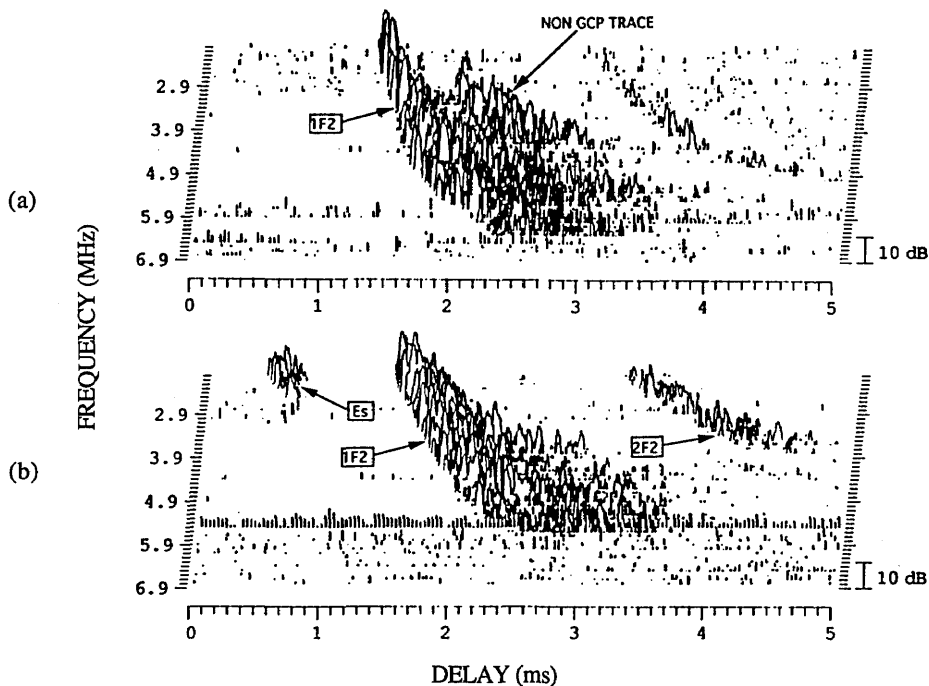

Fig. 14 — Nighttime ionograms, May 13, 1988, (a) Experiment 31, 0900 UT,
(b) Experiment 33, 1100 UT; delay origin = 0.5 ms
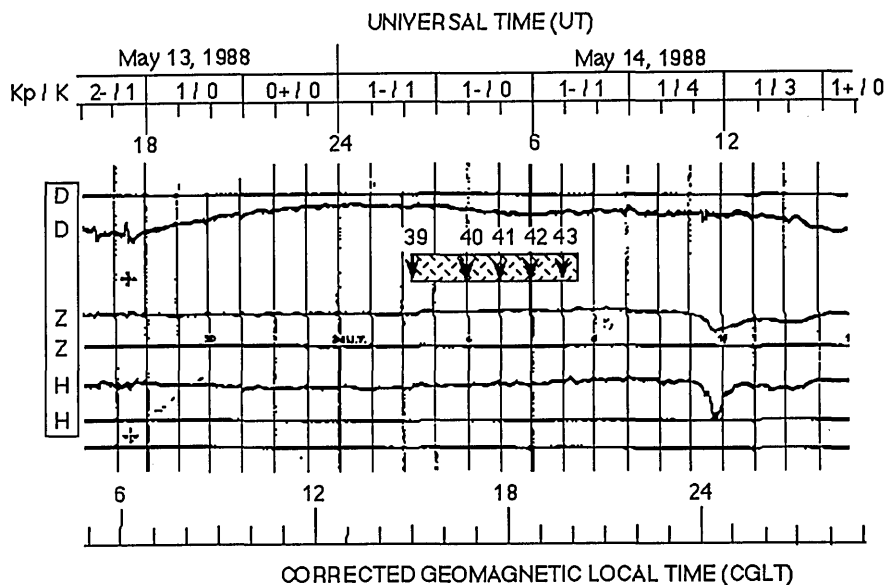
UNIVERSAL TIME (UT)

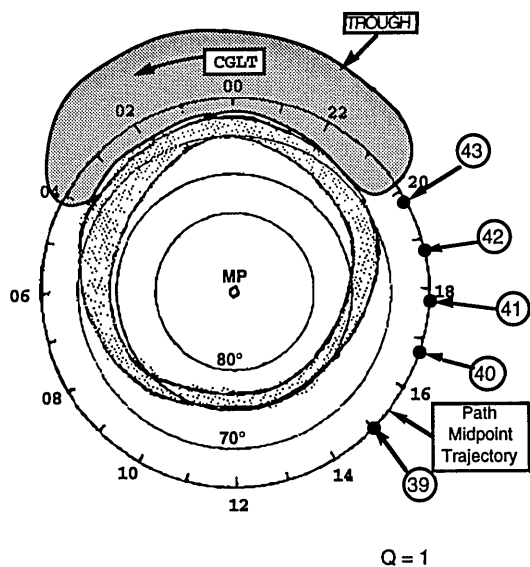Fig. 15(a) — Magnetogram and magnetic disturbance indices relevant to Experiments 39 to 43

Fig. 15(b) — Position of path midpoint relative to oval and trough for Experiments 39 to 43 and for disturbance index Q = 1
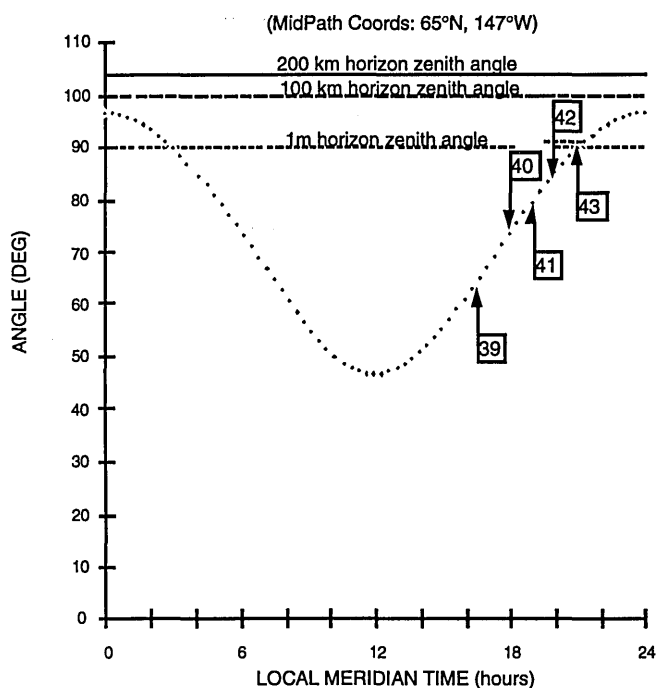
Fig. 15(c) — Solar zenith angles for Experiments 39 to 43

Ionograms for Experiments 34 and 35 (not shown here) show evidence of strong absorption. In Experiment 34, which occurred during the buildup phase of the negative magnetic perturbation, the ionogram trace is barely visible. In Experiment 35, which occurred during the decay phase of the magnetic perturbation, the trace is somewhat recovered, but weak and only visible at frequencies above 3.5 MHz. It is evident that the event that was responsible for the magnetic perturbation also contributed to enhanced D layer ionization, which resulted in the observed absorption event. The time of this event corresponds to a period when the 1 to 10 keV and >40 keV precipitation regions overlap spatially, which may explain the simultaneous occurrence of strong magnetic and absorption events.

An ionogram for Experiment 36 (not shown here) shows a weak, nighttime sporadic E layer return as well as a weak, diffuse F2 layer return indicating that absorption has subsided. The character of the F2 layer signal suggests that the return was spread during the absorption event but was in the process of recovery during Experiment 36. Experiments 37 and 38 show evidence of a gradually recovering ionosphere, as the zenith angle declines from 80° to 70° (Fig. 13(c)), culminating in well-defined E, F1, and F2 layer traces, with little evidence of a scattered signal, in Experiment 38.

4.1.7 Measurements of May 14, 1988, 0215 to 0730 UT (Experiments 39 to 43)

This measurement set was conducted during afternoon to late evening hours (1615 to 2130 LMT, 1500 to 2015 CGLT) and was part of a ground-based, radio-wave ionospheric heating experiment. Insofar as channel spread characteristics are concerned, these results are not included with those of the other experiments because of the effects of ionospheric heating. General observations derived from this channel are assumed to be applicable to the unheated channel, however, since the ionospheric heating did not produce changes in the gross characteristics of the ionosphere.

Magnetic conditions were quiet throughout the measurement interval with K_p values of 1- and local K values fluctuating between 0 and 1. A magnetogram illustrating the quiescent nature of the magnetic conditions is shown in Fig. 15(a). The position of the propagation path midpoint during this series of experiments is subauroral and pre-trough as illustrated in Fig. 15(b). The SZA for this series of experiments is shown in Fig. 15(c), which indicates the afternoon and evening character of the measurements.

All of the ionograms for this measurement set show normal E and F layer traces with no evidence of scatter or multipath returns (other than multihop) or absorption. This is illustrated in the ionogram of Fig. 16, which was made during Experiment 41. The results are very similar to those of Experiments 23 to 29 (Section 4.1.5), which were obtained under almost identical magnetic, midpath, and SZA conditions. The only difference occurs in the first experiment of each group (23 and 39), ·where the F1 layer is more prominent in Experiment 23 than in Experiment 39.
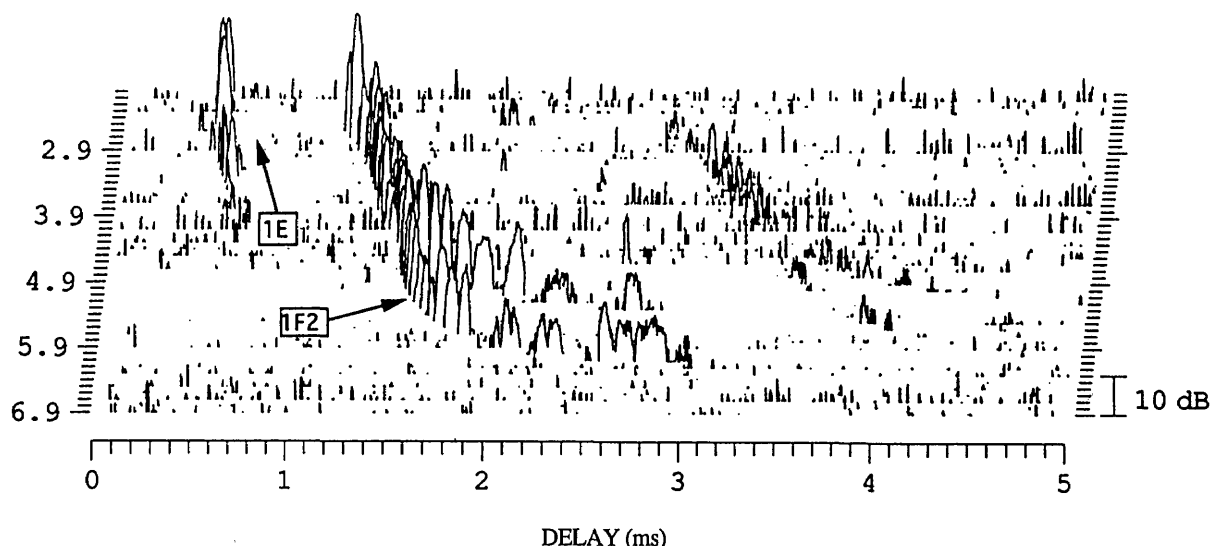
Fig. 16 — Late afternoon ionogram, Experiment 41, May 14, 1988, 0500 UT, delay origin = 0.5 ms

4.1.8 Measurements of May 15, 1988, 0200 to 0830 UT (Experiments 44 to 50)

This series of experiments consisted of late afternoon to late evening measurement times (1600 to 2230 LMT, 1445 to 2115 CGLT). Magnetic conditions during this series of experiments were varied, as can be seen in the magnetogram of Fig. 17(a). Relatively quiet conditions prevailed during the first two experiments of the group, at which time K_p and K were 1+ and 1, respectively. The following three hour interval, which included Experiments 46 and 47, was characterized by magnetic indices of $K_p = 3$ and K = 4. These indices were associated with a large positive fluctuation of the H component of the magnetic field as well as strong fluctuations of the other components. The period following the magnetic perturbation (Experiments 48 to 50) was relatively quiet with a K_p index of 2- and a K index of 2. This group of experiments is important because it illustrates the effect of a magnetic disturbance on the high-latitude ionosphere when the propagation path is subauroral.

The location of the path midpoints relative to the main auroral features is shown in Fig. 17(b). The auroral oval and trough regions are drawn for a Q value of 4 to simulate conditions at the time of the magnetic perturbation. Prior to that time (Experiments 44, 45, and early 46), the midpath points are seen to be at least 5° south of the southern boundary of the auroral oval. At the time of Experiment 47, the midpath point of the path is approximately 4° south of the auroral oval and would be on the order of 3° distant from the southern border of the oval if a Q value of 6 were assumed. Furthermore, the trough region is seen to be irrelevant to Experiment 47 since the experiment was conducted approximately 3 hours before an overhead trough condition. The midpath points for Experiments 48 and 49 continue to be subauroral and unaffected by the trough region while that for Experiment 50 appears to be at the auroral-trough boundary. If a value of Q appropriate to conditions during Experiments 48 to 50 were used to define the oval and trough regions of Fig. 17(b) (i.e., Q = 2), then the midpath point for Experiment 50 would also be subauroral and would lie within the nominal trough region rather than at the oval-trough boundary.

Figure 17(c) shows the SZA curve for this series of experiments. It indicates that, were it not for the effect of the magnetic disturbance, the ionograms for this set of measurements would have been characterized by the dominance of a normal F1 layer in the early experiments, and dually give way to dominance by a normal F2 layer in the later experiments.

Fig. 17(a) — Magnetogram and magnetic disturbance indices relevant to Experiments 44 to 50
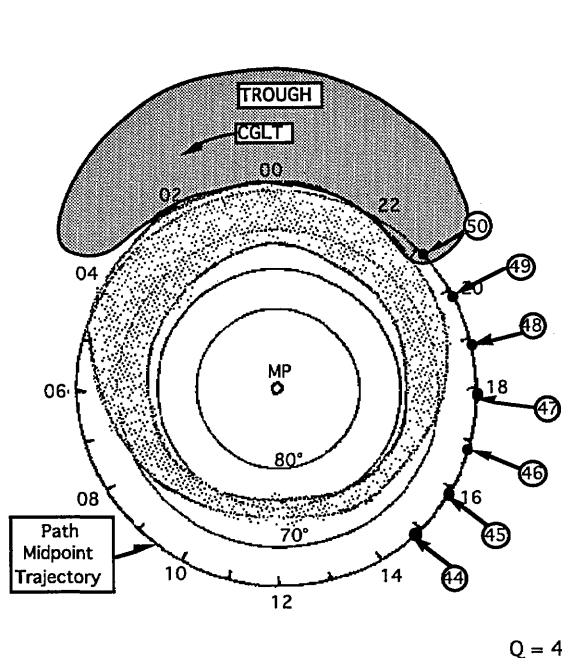
Fig. 17(b) — Position of path midpoint relative to oval and trough for Experiments 44 to to 50 and for disturbance index Q = 4
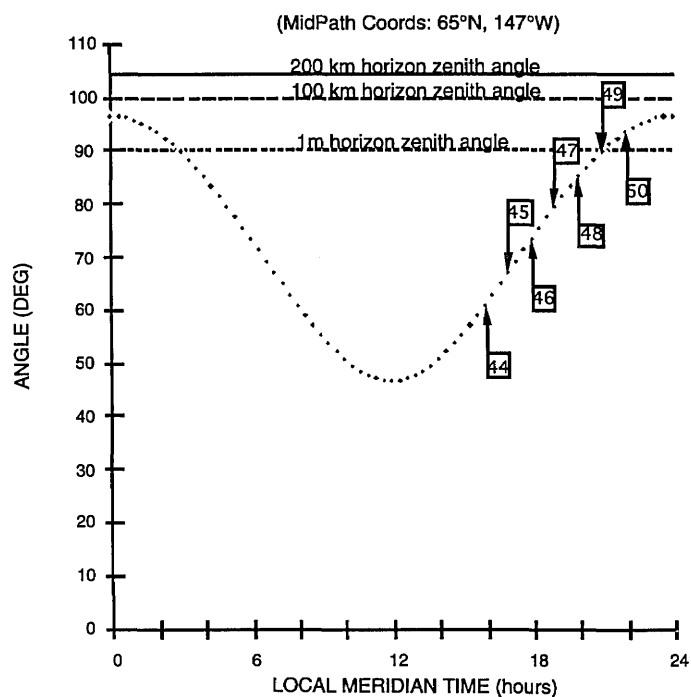
Fig. 17(c) — Solar zenith angles for Experiments 44 to 50
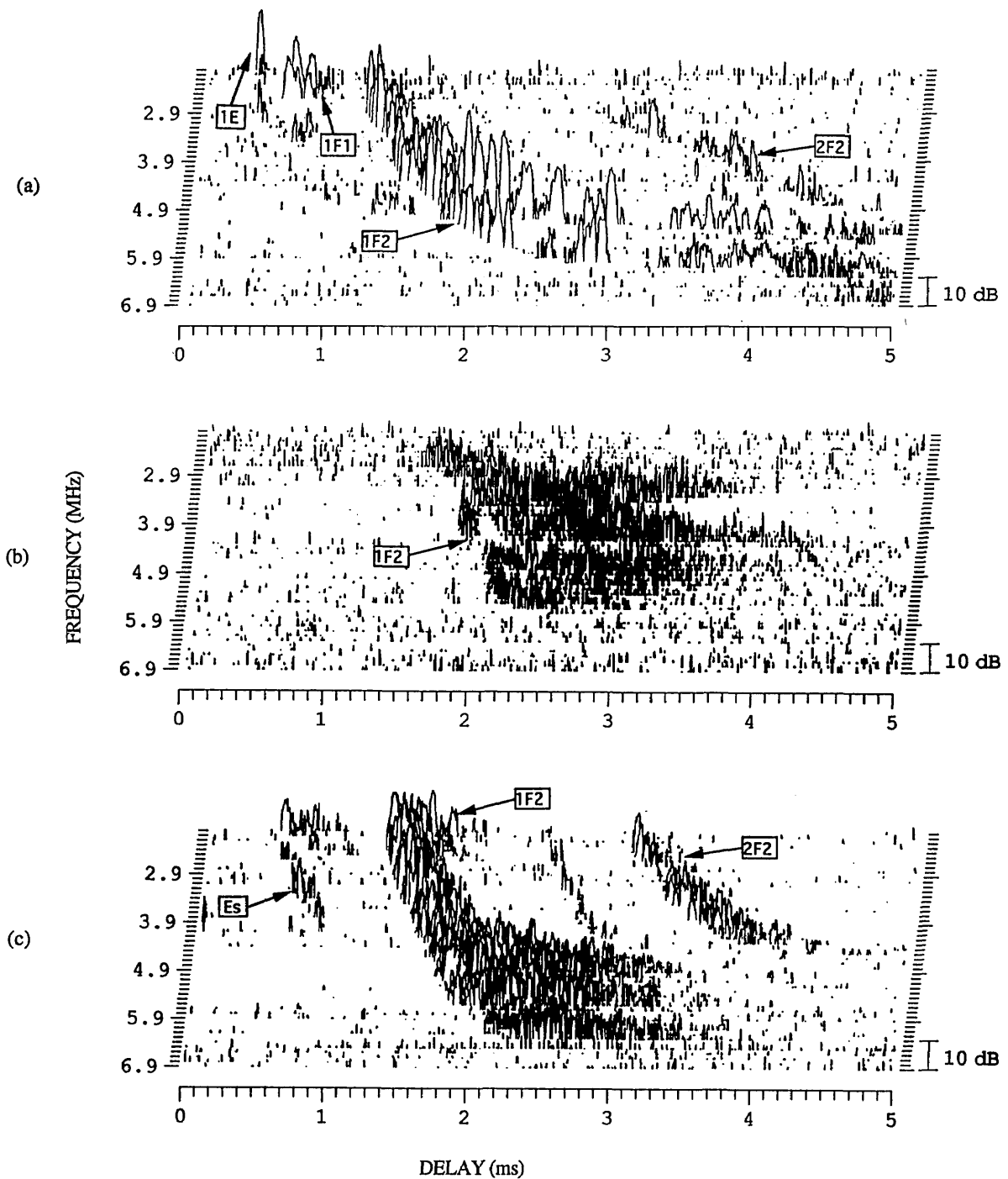
Fig. 18 — Late afternoon/evening ionograms, May 15, 1988. (a) Experiment 46, 0400 UT,
(b) Experiment 47, 0500 UT, (c) Experiment 48 0600 UT; delay origin = 0.5 ms

The ionograms for Experiments 44 and 45 were typical of magnetically quiet, daytime conditions. The initial ionogram for Experiment 46 (Fig. 18(a)) was also typical of undisturbed daytime conditions with no evidence of spread F. Clear signs of the onset of spread F began to appear early in the probing period of Experiment 46 but were quickly masked by an absorption event that was centered on the peak of the magnetic perturbation.

Absorption had apparently subsided by the time of the start of Experiment 47, revealing a very weak and diffuse spread F ionogram trace (Fig. 18(b)). Ionograms for post-perturbation experiments (Experiments 48, 49, and 50) showed evidence of range-spread spread F (e.g., Fig. 18(c), Experiment 48). The signal levels for Experiments 48 to 50 were much higher than those of Experiment 47, and their ionogram traces were primarily irregular rather than diffuse.

These observations are interesting because they clearly illustrate a case in which spread F occurs in association with an isolated magnetic perturbation on a path well south of the auroral oval. As previously discussed, auroral precipitation events that directly affect the F layer are confined to the region of the auroral oval. Furthermore, at 1700 to 1800 CGLT, precipitation events affecting E layer conductivity, and associated magnetic field perturbations, are primarily confined to the auroral oval with some subauroral spillover. Allowing for some diffuse precipitation beyond the boundary of the auroral oval, we estimate that the southernmost boundary of the E layer precipitation region is approximately 3° north of the propagation path, which is equivalent to a lateral displacement of approximately 370 km. E layer currents at that distance could account for the observed magnetic fluctuation at College Alaska but it is also possible that the magnetic event is the result of an isolated surge in the global ring current. The absorption event must be due to an enhancement of the high energy (>40 keV) electron flux associated with the diffuse aurora.

The observed spread F could be a result of the modification of the overhead ionosphere or of sidescatter from an irregularity region located within the oval. An examination of trace delays for this group of experiments shows an increase of approximately 400 μs between the start of Experiments 46 and 47, out of a total trace delay time of approximately 1.65 ms. Scattering from an irregularity region within the auroral oval would require a trace delay increase of approximately 1.1 ms and may therefore be ruled out. The observed delay variation can be readily explained, however, in terms of a vertical rise and fall of the overhead layer. An increase of approximately 55 km in the virtual height of the layer (from an initial value of 245 km), is sufficient to explain the observed increase in delay between Experiments 46 and 47. Evidence of vertical transport of ionization in the auroral ionosphere in association with magnetic disturbances has been cited by Bates and Hunsucker (1974). Rapid vertical motion of this kind could trigger an instability leading to the observed spread F. Subsequent ionogram traces (Experiments 48 to 50) show a gradually decreasing trace delay until, at the start of Experiment 50 (roughly 4 hours later), the delay has reverted to its value at the start of Experiment 46.

Based on the character of the ionograms (Figs. 18(b) and 18(c)), one should expect substantially enhanced channel spread parameters for Experiments 47 through 50. These results are considered in greater detail in Section 4.2.3.

UNIVERSAL TIME (UT)
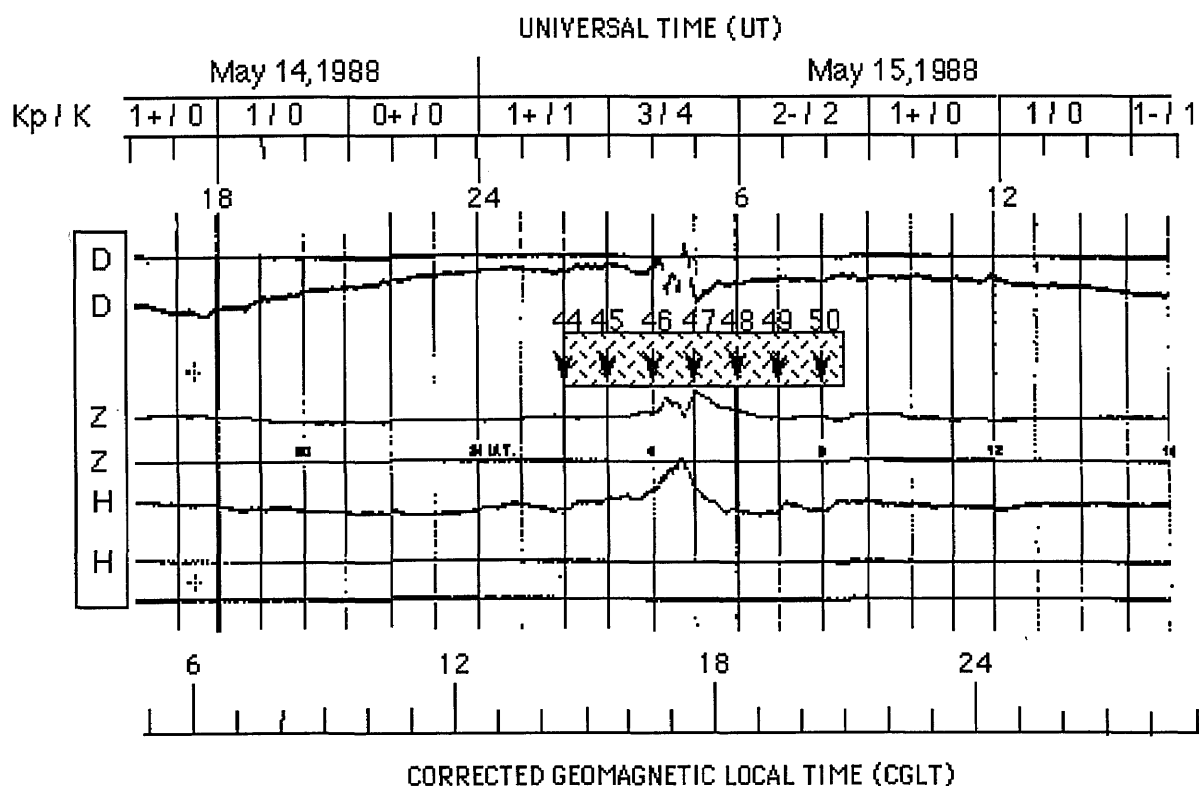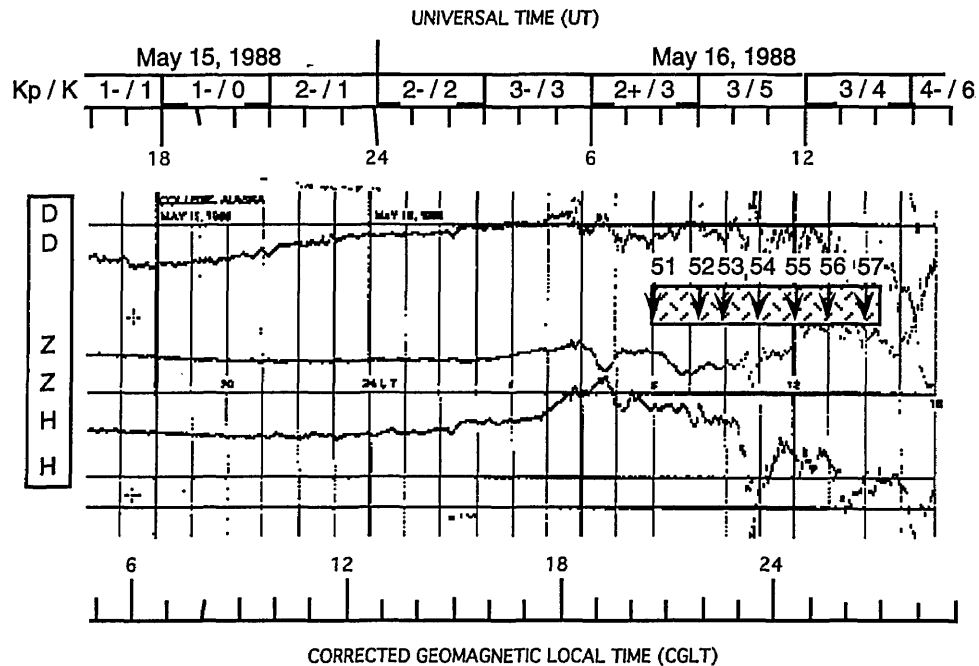

Fig. 19(a) — Magnetogram and magnetic disturbance indices relevant to Experiments 51 to 57
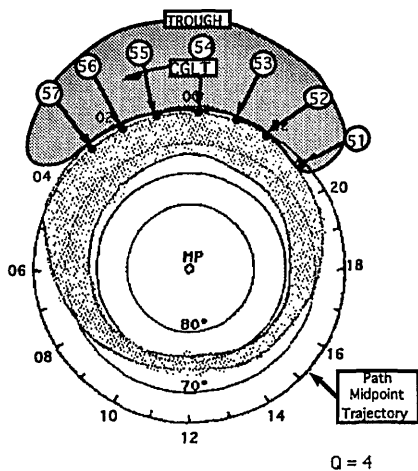

Fig. 19(b) — Position of path midpoint to oval
and trough for Experiments 51 to 57 and for dis-
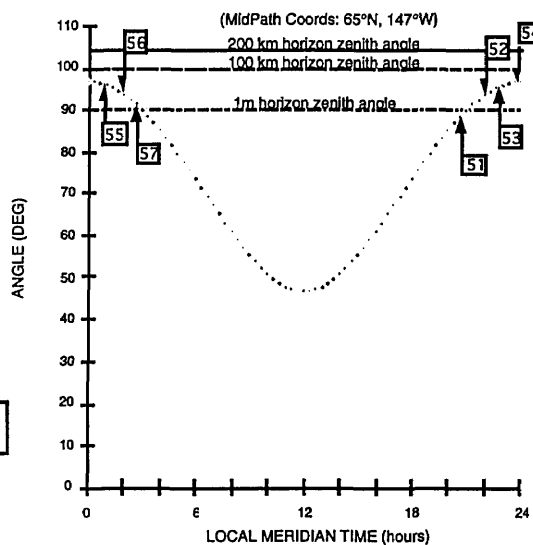turbance index Q = 4

Fig. 19(c) — Solar zenith angles for
Experiments 51 to 57

4.1.9 Measurements of May 16, 1988, 0800 to 1430 UT (Experiments 51 to 57)

This was a nighttime measurement set (2200 to 0430 LMT, 2045 to 0315 CGLT), which coincided with a magnetospheric substorm. It therefore is expected to present the most difficult conditions for HF skywave propagation on the channel. The magnetogram describing magnetic conditions during this set of measurements is shown in Fig. 19(a). The K_p index during this period varied between 2+ and 3, while the local K index varied between values of 3 and 5. As can be seen from the magnetogram, all of the experiments were conducted during disturbed conditions but the worst conditions were experienced during Experiments 53 to 57. Because this represents an extreme set of conditions, it is considered in greater detail in Section 4.2.4.

A value of Q = 4 was selected as the magnetospheric disturbance index for representing the position and size of the auroral oval and the trough in Fig. 19(b). As can be seen from this figure, the midpath points for all of the experiments lie in the nighttime sector either within the oval or on the oval-trough boundary. It is important to note that all energy regimes for precipitating electrons overlap in the nighttime auroral oval, as do the regions of the discrete and diffuse aurora. This is especially significant during magnetically disturbed periods.

The curve of SZA vs LMT (Fig. 19(c)) indicates that all measurements, except for those of Experiment 51, occurred at solar zenith angles greater than 90° (post-ground-sunset), while the SZA for Experiment 51 was approximately 88°. The significance of these large zenith angles is that direct solar effects (photoionization in the E and F1 layers) should be minimal.

The ionogram for Experiment 51 (not shown here) shows evidence of an irregular trace at a group delay of 1.2 ms, corresponding to a virtual height of 175 km. Elevated layers and unusual vertical profiles of electron density at auroral latitudes have been previously reported by Bates and Hunsucker (1974), especially during magnetically disturbed conditions. The ionogram for Experiment 52 (Fig. 20(a)) shows fully developed (one hop) blanketing sporadic E at all frequencies (2 to 7 MHz) with indications of multiple layers and a 2-hop E_s return. The height of the lowest of the multiple layers is estimated to be 110 km. Experiment 53, which starts before but continues through the start of the main phase of the magnetic storm, shows a weaker, range-spread E_s return as well as a weak, diffuse F2 layer return (Fig. 20(b)). In Experiment 54, which coincides with a very large negative perturbation of the H component of the magnetic field, absorption is a dominant factor. At this time, no F layer returns are visible, and E_s layer returns are visible only above approximately 5.8 MHz. In Experiments 55 and 56, the absorption event appears to have subsided and E_s and spread F returns reappear. This is illustrated by the ionogram for Experiment 56 (Fig. 20(c)). During Experiment 57, no returns were visible, implying the resumption of enhanced auroral absorption with accompanying radio blackout.

Comparison of these results with those of Experiments 30 to 36 (Section 4.1.6) is of interest because they correspond to nearly identical test conditions except for the degree of magnetic disturbance. In both sets of measurements, enhanced absorption is associated with the occurrence of a large, discrete, magnetic perturbation. In the case of magnetic storm conditions (Experiments 51 to 57), strong sporadic E is more prevalent (an indication of overhead E layer effects), and the spread F traces appear to be more diffuse in character. Our experience with these kinds of measurements is that the more diffuse returns are characterized by broader Doppler-spreads. Cursory examination of the scattering functions for Experiments 51 to 57 indicates that Doppler-spreads of approximately 15 Hz are observed. More details regarding these spread parameters are provided in Section 4.2.
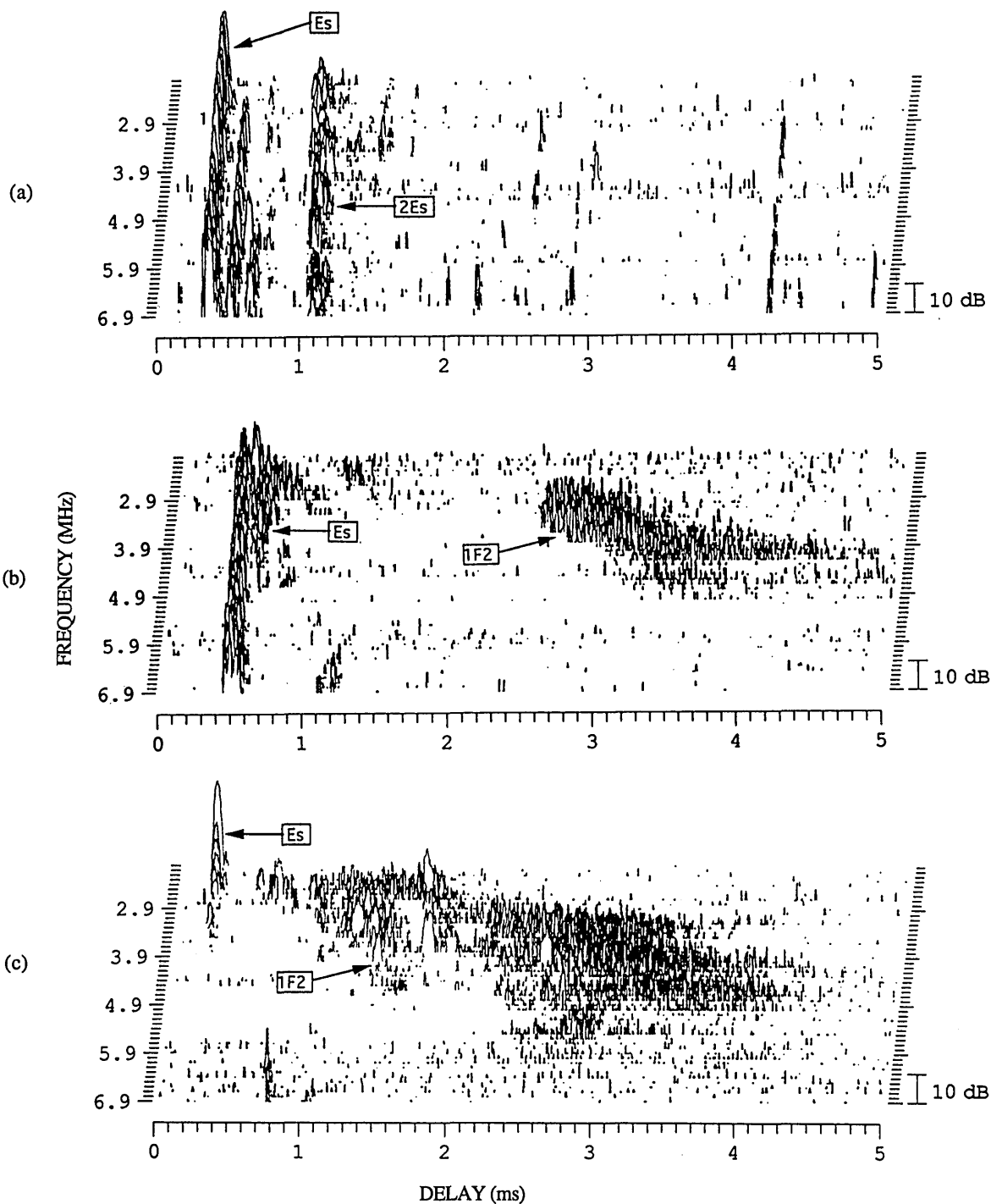
Fig. 20 — Nighttime ionograms, May 16, 1988. (a) Experiment 52, 0915 UT, (b) Experiment 53, 1000 UT, (c) Experiment 56, 1300 UT; delay origin = 0.5 ms

4.2 Channel Spread Parameters for the NVIS High-latitude Channel

The characteristics of the high-latitude channel are critically dependent on the location of the skywave propagation path relative to the auroral oval and on the severity of auroral disturbance conditions. In this section, four sets of measurements representing a broad range of environmental conditions are considered. In each case, the channel scattering function is examined. Parameters derived from the channel scattering function include signal amplitude, delay-spread, Doppler-spread, and the channel spread factor. The four cases considered are (a) magnetically quiet daytime conditions, (b) magnetically disturbed daytime conditions, (c) magnetically quiet nighttime conditions, and (d) magnetically disturbed nighttime conditions.

4.2.1 *Magnetically Quiet Daytime Conditions*

During this measurement campaign, magnetically quiet daytime conditions were encountered on four separate occasions. General results for these cases, including ionograms, are presented in Sections 4.1.1, 4.1.4, 4.1.5, and 4.1.6. Generally speaking, the signal amplitude and spread parameters for all of these measurements were comparable and typical of the quiet, daytime high-latitude channel. Some differences were noted in the delay-spread depending on the time of day of the measurements. These differences were a result of enhanced dispersive effects due to the presence of the F1 layer. The smallest values of the spread parameters were observed during magnetically quiet, late afternoon conditions, as exemplified by those described in Section 4.1.5 (e.g., Experiment 27). Spread parameters for Experiment 27 are examined in detail in this section and are used as a benchmark for assessing the performance of the channel under less ideal conditions.

The measurements of Experiment 27 were made at a location that was approximately 7° ($\approx$865 km) south of the southernmost boundary of the auroral oval (Fig. 11(b)). The ionogram for this measurement (Fig. 12) shows well-defined E and F2 layer traces and no evidence of an F1 layer trace. Figure 21 shows an example of the scattering function for the 1F2 return for Experiment 27 at a frequency of 2.8 MHz (a feature of this scattering function, labeled spurious on the figure, is an artifact of the hardware). The scattering function is comparable to that which would be observed on a quiet, daytime, midlatitude channel. Calculated values of all parameters for this frequency are shown on the plot. The measured delay and Doppler-spreads for 2.8 MHz are negligible and of the order of the measurement resolution. At frequencies closer to the layer critical frequency, delay dispersion increases, leading to larger values of delay-spread and smaller values of signal amplitude. Signal characteristics for this experiment, averaged over all frequencies, are summarized in Table 2 at the end of Section 4.

4.2.2 *Magnetically Disturbed Daytime Conditions*

Measurements involving disturbed daytime conditions include those described in Sections 4.1.2 and 4.1.8. Of these two cases, the best data were obtained for the measurements of 15 May 1988, which are briefly discussed in Section 4.1.8. As shown in Fig. 17(a), the magnetic perturbation was an isolated one of roughly 90 minutes duration occurring in the late afternoon. The measurements of primary interest to this case are those of Experiments 46 and 47 and subsequent experiments (48 to 50), which describe post-perturbation conditions. A discussion of these events can also be found in an *IEE Conference Proceedings* publication (Wagner and Goldstein 1991).

As mentioned in Section 4.1.8, results for Experiment 46 indicate a normal daytime ionogram for the pre-perturbation period (Fig. 18(a)). During the subsequent probing period of Experiment 46, signal was visible for the first 5 minutes but was followed by a period of "radio blackout" that

DELAY
(us)

PEAK AMPLITUDE = 64 dB

2σ DOPPLER-SPREAD = .07 Hz

2σ DELAY-SPREAD = 3 μs
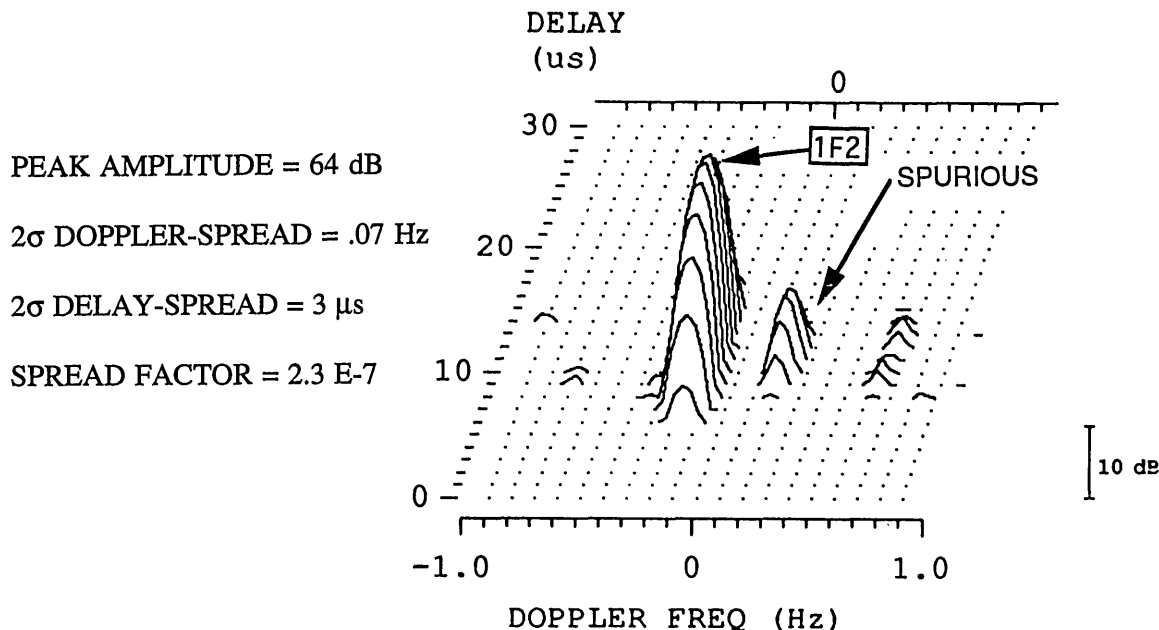
SPREAD FACTOR = 2.3 E-7

DOPPLER FREQ (Hz)

Fig. 21 — F layer scattering function for magnetically quiet daytime conditions, Experiment 27,
12 May 1988, frequency = 2.8 MHz, delay origin = 1.735 ms

persisted for the remainder of the measurement period. Unfortunately, the magnetic perturbation was unexpected and the data sampling rate used in Experiment 46 was too slow for the rapid signal fluctuation rate that was encountered. Spectral aliassing made an accurate estimate of the spread parameters for the period prior to the absorption event impossible. Nevertheless, the rapid fade rate was a good indication that spread F was very likely to be present.

The measurements of Experiment 47 coincided with the decay phase of the magnetic perturbation (Fig. 17(a)). The absorption effects noted in Experiment 46 had subsided, revealing a strongly scattered signal as indicated by the severe spread F ionogram of Fig. 18(b). It is conjectured that were it not for the absorption event and the inadequate sampling rate of Experiment 46, similar effects would have been observed in that measurement.

Scattering functions for Experiment 47 revealed extensive delay- and Doppler-spreads. Figure 22 shows an example of an F layer scattering function for the channel at a frequency of 3.8 MHz in the form of a contour plot of signal amplitude, in dB, relative to the peak value of the scattering function (plotted contour levels are listed alongside the plot). For each feature in this plot (and for all succeeding contour plots), the value of the outermost contour is equal to the lowest listed contour level. It is clear from the figure that the signal has been extensively spread in delay and in Doppler as a result of propagation via the ionospheric channel. In fact, the Doppler window for this case (±8 Hz) is seen to be not quite wide enough to fully accommodate the Doppler-spread of the signal without aliassing. Calculated values for the scattering function peak amplitude, the delay- and Doppler-spreads, and the spread factor at this frequency are shown on the figure. Table 2 presents an average of these parameters over all frequencies. Note that the estimate of the Doppler-spread for this case is probably lower than its true value because of aliassing.

PEAK AMPLITUDE = 33 dB

2σ DOPPLER-SPREAD = 7 Hz

2σ DELAY-SPREAD = 1133 μs

SPREAD FACTOR = 8 E-3
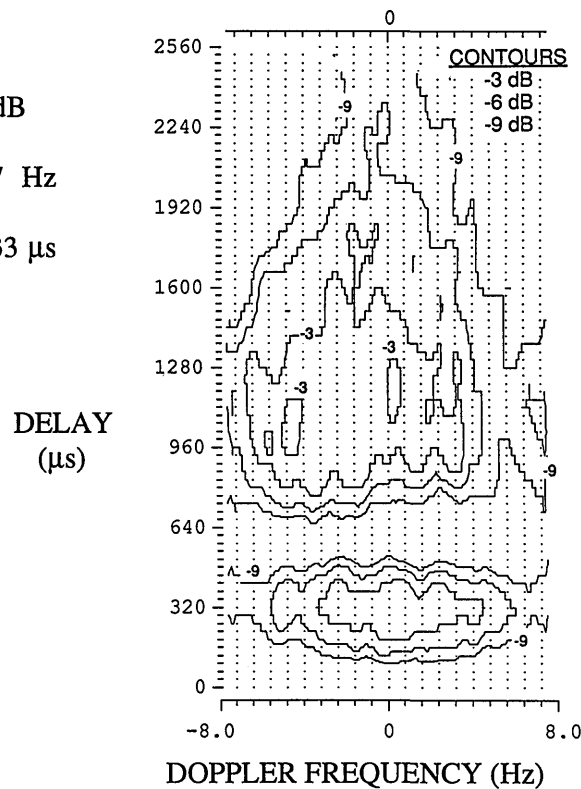
DELAY
(μs)

DOPPLER FREQUENCY (Hz)

Fig. 22 — F layer scattering function for magnetically disturbed daytime conditions, Experiment 47, 14 May 1988, frequency = 3.8 MHz, delay origin = 1.79 ms

Experiments 48 to 50, all of which were post-perturbation measurements, show evidence of an irregular ionosphere in the form of range-spread spread F ionograms (e.g., Fig. 18(c)). They differ from Experiment 47, however, in that the delay-spread of their ionograms is not as severe as that of Experiment 47, except near the F layer critical frequency. Furthermore, signal amplitude is substantially larger and Doppler-spreads are substantially smaller than for Experiment 47. This is clearly illustrated by comparing a scattering function for Experiment 48 (Fig. 23) with that of Experiment 47 (Fig. 22). Figure 23 is a scattering function for a frequency of 3.3 MHz showing what appears to be a slant sporadic E return (early feature) and a 1F2 return (later feature). Derived values of all channel parameters for the F2 layer return at this frequency are indicated on the figure. Values of the peak signal amplitude and the spread parameters, averaged over all frequencies and measurement repetitions, are presented in Table 2.

4.2.3 Magnetically Quiet Nighttime Conditions

Magnetically quiet nighttime conditions were encountered on only one occasion during this measurement series. The measurements of 13 May 1988, involving Experiments 30 to 38, were conducted on a night when magnetic conditions were quiet at the start of the measurements but deteriorated midway through the measurement series as discussed in Section 4.1.6. Magnetically quiet conditions prevailed during Experiments 30 to 33. This section examines signal amplitude and spread characteristics for Experiments 31 and 33.

Contours

-5 dB
-10 dB
-15 dB
-20 dB
-25 dB
-30 dB

1F2 RETURN

PEAK AMPLITUDE = 56 dB

2σ DOPPLER-SPREAD = 0.5 Hz

2σ DELAY-SPREAD = 139 μs
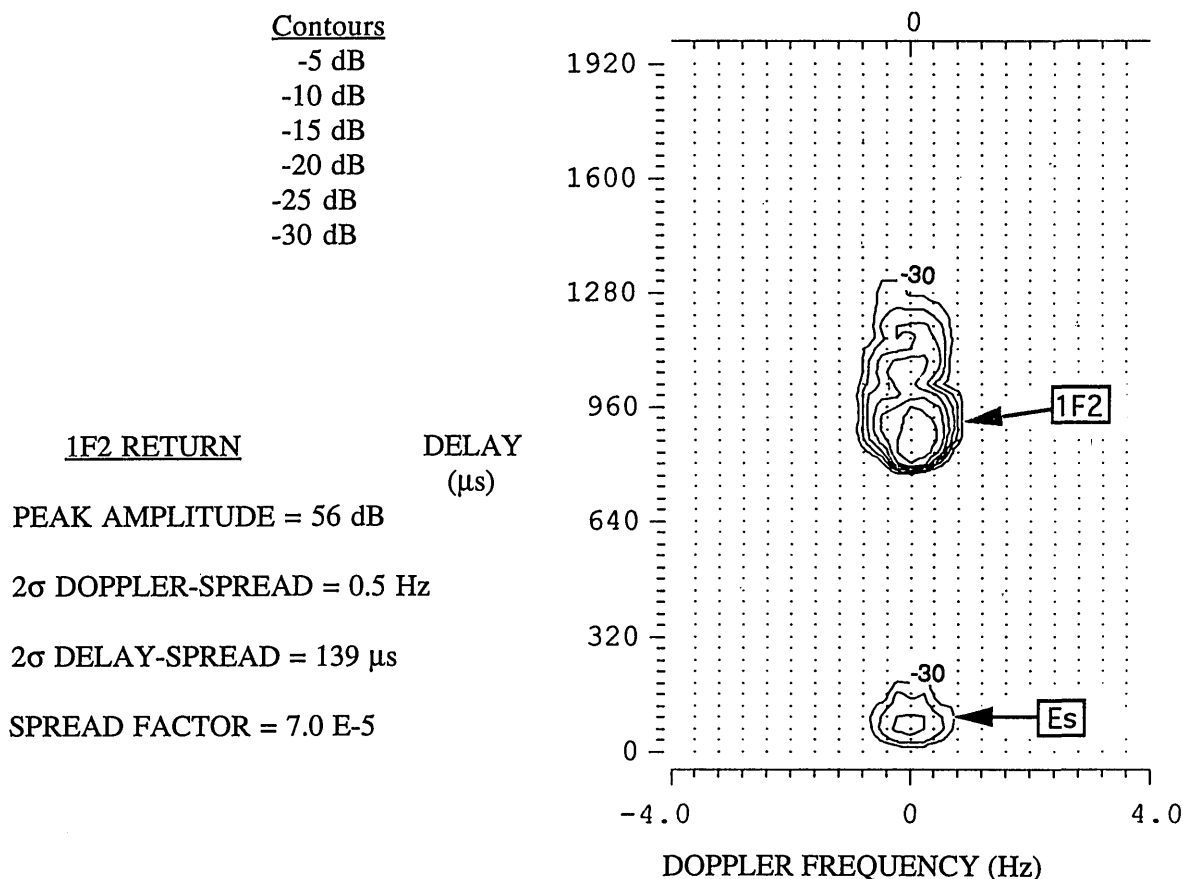
SPREAD FACTOR = 7.0 E-5

DELAY
(μs)

Fig. 23 — Scattering function for post-perturbation, daytime conditions, Experiment 48,
14 May 1988, frequency = 3.3 MHz, delay origin = 0.852 ms

Start times for Experiments 31 and 33 were separated by two hours (2145 and 2345 CGLT), with the result that the midpath point for Experiment 31 was subauroral (by about 2° of latitude) while that of Experiment 33 was on the trough-auroral boundary (Fig. 13(b)). These differences in location appear to have contributed to differences in the nature of the propagation conditions. In Experiment 31, the ionogram (Fig. 14(a)) indicates the presence of a normal looking overhead trace, which becomes somewhat irregular at frequencies near the F layer critical frequency, plus a delayed return that can reasonably be attributed to "side" reflection from irregularities at or near the southern boundary of the auroral region. The ionogram (Fig. 14(b)) for Experiment 33, on the other hand, is a classic range-spread spread F ionogram.

Figure 24 shows a contour plot of a scattering function for Experiment 31 at a frequency of 3.3 MHz. The scattering function shows the presence of two separate returns, one for the overhead reflection and another for the oblique reflection from an irregularity region situated in the vicinity of the oval-trough boundary. Values of peak signal amplitude and spread parameters for this case are shown on the figure. They indicate that the signal amplitude is strong enough to be construed as a reflected signal but that the spread parameters are sufficiently large that they indicate a multipath-reflected signal rather than a simply-reflected signal. It should be noted that the presence of the two separate returns tends to increase the measured 2σ values of the spread parameters.

Contours
-5 dB
-10 dB
-15 dB
-20 dB
-25 dB
-30 dB

DELAY
(μs)

PEAK AMPLITUDE = 57 dB

2σ DOPPLER-SPREAD = 1.0 Hz

2σ DELAY-SPREAD = 415 μs

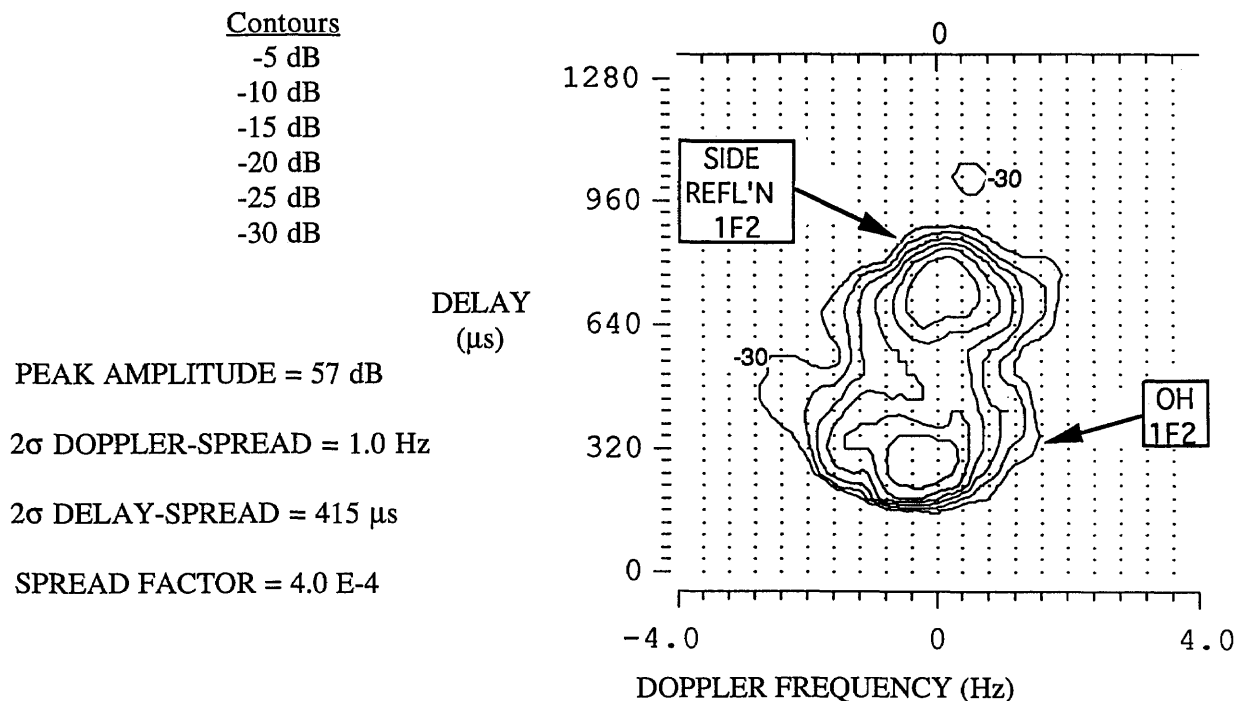SPREAD FACTOR = 4.0 E-4

DOPPLER FREQUENCY (Hz)

Fig. 24 — F layer scattering function for magnetically quiet nighttime conditions, Experiment 31, 13 May 1988, frequency = 3.3 MHz, delay origin = 1.748 ms

Figure 25 shows a scattering function for the case of Experiment 33 at a frequency of 3.3 MHz. The signal amplitude for Experiment 33 tends to be somewhat smaller than for Experiment 31 but the spread parameters are comparable. Parameters for this scattering function are shown on the figure.

Table 2 includes averages over all frequencies and measurement repetitions of signal amplitude and spread parameters for Experiments 31 and 33.

4.2.4 Magnetically Disturbed Nighttime Conditions

Measurements involving disturbed nighttime conditions include those described in Sections 4.1.3 and 4.1.9. The measurements described in Section 4.1.3 consist of postmidnight and early morning measurement times, where only the postmidnight measurements would have been relevant to the present discussion. These were of little value, however, because of strong absorption and blanketing ·sporadic E conditions that prevailed during that entire period.

The measurements described in Section 4.1.9 pertain to a period during which the propagation path was located within a longitudinal sector centered on CGLT midnight and at the latitude of the oval-trough boundary (Fig. 19(b)). Furthermore, these measurements coincided with a period of strongly disturbed magnetic conditions (Fig. 19(a)). In spite of intermittent periods of strong radiowave absorption and blanketing sporadic E, these measurements included extended periods during which F layer returns were visible. This section discusses F layer signal characteristics obtained during these periods, particularly those derived from Experiments 53 and 56.

Contours
-5 dB
-10 dB
-15 dB
-20 dB
-25 dB

DELAY
(μs)

PEAK AMPLITUDE = 52 dB

2σ DOPPLER-SPREAD = 0.64 Hz

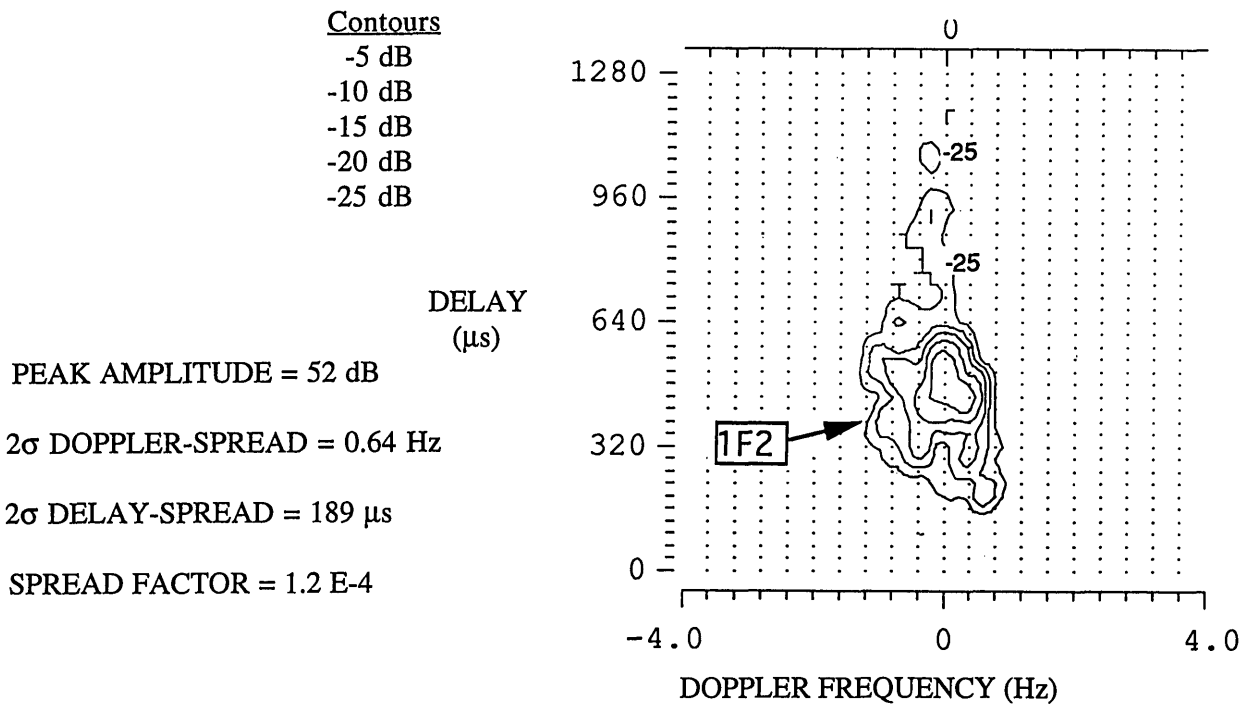2σ DELAY-SPREAD = 189 μs

SPREAD FACTOR = 1.2 E-4

Fig. 25 — F layer scattering function for magnetically quiet nighttime conditions, Experiment 33, 13 May 1988, frequency = 3.3 MHz, delay origin = 1.972 ms

The start of Experiment 53 coincided with a period of relative magnetic calm approximately 15 minutes before the magnetic storm main-phase negative perturbation. The measurements continued through the early part of the main-phase perturbation. The ionogram made just prior to the start of the experiment (Fig. 20(b)) showed strong evidence of a range-spread E_s return with a blanketing frequency of approximately 3 MHz. Above the blanketing frequency, a weak, diffuse, range-spread F layer return was visible. A scattering function for a frequency of 4.2 MHz made during the early part of the storm main phase is shown in Fig. 26 along with signal characteristics derived from the scattering function. The results indicate substantial delay- and Doppler-spread as well as a weak signal amplitude as might have been inferred from the ionogram. Table 2 includes an average of the channel parameter values, taking account of all frequencies used and all measurement repetitions.

Experiment 56 was conducted after the main-phase perturbation but at the start of a second steep decline in the value of the H component of the magnetic field perturbation. The ionogram describing conditions during Experiment 56 (Fig. 20(c)) shows evidence of a sporadic E return up to a frequency of approximately 2.5 MHz, and a diffuse spread F return consisting primarily of weak scatter returns with some embedded reflected returns. Figure 27 shows an example of a scattering function at a frequency of 4.2 MHz along with channel characteristics derived from the scattering function. The signal amplitude and delay-spread derived in this case are comparable to those derived for the case of Experiment 53 (Fig. 26), but the Doppler-spread is larger by about a factor of 2. Table 2 presents average values for the amplitude and spread parameters.
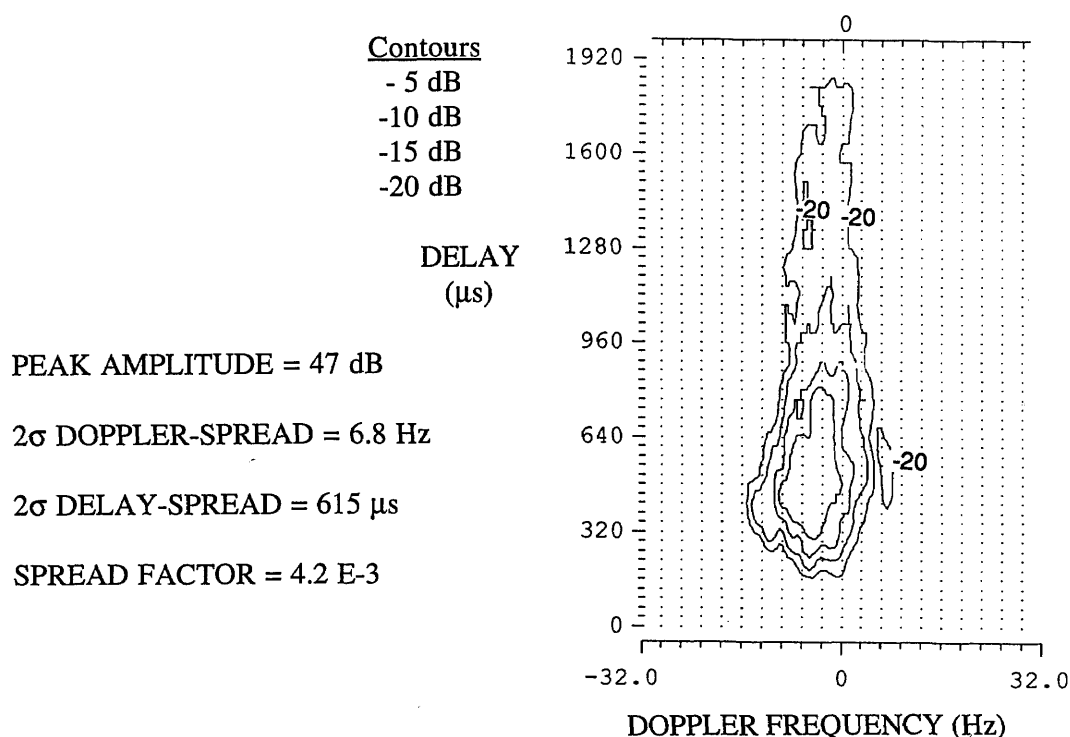
Contours
- 5 dB
-10 dB
-15 dB
-20 dB

DELAY
(μs)

PEAK AMPLITUDE = 47 dB

2σ DOPPLER-SPREAD = 6.8 Hz

2σ DELAY-SPREAD = 615 μs

SPREAD FACTOR = 4.2 E-3

DOPPLER FREQUENCY (Hz)

Fig. 26 — One-hop F layer scattering function for magnetically disturbed nighttime conditions,
Experiment 53, 16 May 1988, frequency = 4.2 MHz, delay origin = 2.996 ms

Contours
-5 dB
-10 dB
-15 dB
-20 dB

DELAY
(μs)

PEAK AMPLITUDE = 45.5 dB

2σ DOPPLER-SPREAD = 15.8 Hz

2σ DELAY-SPREAD = 744 μs
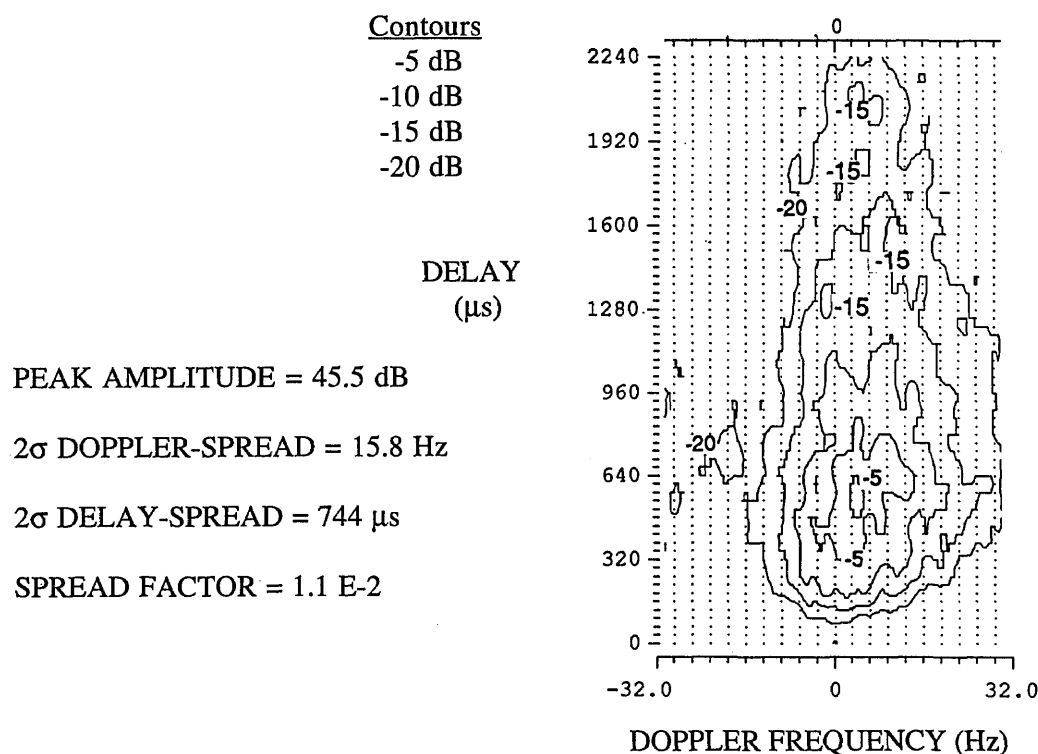
SPREAD FACTOR = 1.1 E-2

DOPPLER FREQUENCY (Hz)

Fig. 27 — One-hop F layer scattering function for magnetically disturbed nighttime conditions,
Experiment 56, 16 May 1988, frequency = 4.2 MHz, delay origin = 2.740 ms

Table 2 — Average Characteristics for the NVIS Channel

Channel Condition	Exp. No.	Amplitude (dB)	Doppler Spread (Hz)	Delay Spread (μs)	Spread Factor
Magnetically Quiet - Daytime (subauroral)	27	52	0.09	80	7.7 E-6
Magnetically Perturbed - Daytime (subauroral)	47	44	6.2	812	5.5 E-3
Post-Perturbation - Daytime (subauroral)	48	62	0.6	545	4.6 E-4
Magnetically Quiet - Nighttime (subauroral)	31	57	1.6	583	1.0 E-3
Magnetically Quiet - Nighttime (auroral)	33	47	0.65	840	5.7 E-4
Magnetically Disturbed - Nighttime (auroral)	53	38.6	7.6	1159	9.2 E-3
Magnetically Disturbed - Nighttime (auroral)	56	42.2	12.6	571	7.5 E-3

5. DISCUSSION

The results listed in Table 2 cover a wide range of ambient conditions from magnetically quiet daytime conditions to magnetically disturbed nighttime conditions. The channel characteristics observed for Experiment 27 (magnetically quiet daytime conditions) represent the best propagation conditions observed during the entire series of measurements. They therefore serve as a benchmark by which to judge the impact of changed conditions as represented by the other cases listed in Table 2. It should be stressed, however, that the measured values of Doppler-spread and spread factor for Experiment 27 are upper bounds rather than accurate estimates of these parameters. This is because the measurement of Doppler-spread, in that case, was limited by the measurement resolution of the instrument.

Magnetically disturbed conditions yield comparable values of signal amplitude and spread parameters regardless of time of day. This is illustrated in Table 2 for Experiments 47, 53, and 56. In all three cases, the spread parameters are within a factor of two of one another, and are two or three orders of magnitude greater than the corresponding parameters for the magnetically quiet daytime case (Experiment 27). Signal amplitudes for these three cases are also substantially smaller than that obtained for the benchmark case. The difference would be even more marked were it not for the amplitude reduction caused by enhanced delay dispersion in Experiment 27. This effect is readily observed in Fig. 29(a) in Section 5.2.

The three remaining cases (i.e., the daytime post-perturbation case (Experiment 48), the nighttime subauroral case (Experiment 31), and the nighttime auroral case (Experiment 33) yield values for the spread parameters that are very close to one another. These measurements were characterized by magnetically quiet conditions and, in the cases of Experiments 33 and 48, by range-spread spread F ionograms. Comparison of these three cases with the magnetically disturbed cases (Experiments 47, 53, and 56) reveals comparable values of delay-spread, but Doppler-spreads and spread factors that are approximately an order of magnitude smaller. A similar comparison with results for the benchmark case (Experiment 27) indicates that the delay and Doppler-spreads for Experiments 31, 33, and 48 are roughly an order of magnitude larger than those of the benchmark case, and their spread factors are approximately two orders of magnitude larger.

Finally, the signal amplitude for the magnetically quiet, nighttime, subauroral case (Experiment 31) is comparable with that of the daytime magnetically quiet cases (Experiments 27 and 48), while

the magnetically quiet, nighttime, auroral path (Experiment 33) yields signal amplitudes that are comparable with those obtained during magnetically disturbed periods. This suggests that scattering rather than reflection of incident signals occurs at all times in the auroral region but only during magnetically disturbed times at subauroral locations. The major difference in channel characteristics between the magnetically quiet and magnetically disturbed auroral regions is in the width of the Doppler-spread, which is significantly greater during disturbed periods. This difference is probably caused by an increased plasma drift velocity during magnetically disturbed periods.

The detailed effects of changes in magnetic conditions and of path location relative to the auroral oval can be better appreciated by graphical means as shown in the scatter plots of Figs. 28, 29, and 30. In each of these figures, peak signal amplitude in dB is plotted against the 2σ Doppler-spread (Fig. 28), the 2σ delay-spread (Fig. 29), and the spread factor (Fig. 30). Each figure consists of two separate graphs, one for daytime measurements and the other for nighttime measurements. In each graph, the measurement points are represented by markers that identify the specific experiment or measurement group and each measurement group is appropriately labeled according to magnetic conditions and location of the propagation path relative to the auroral oval.

5.1 Scatter Plot of Peak Signal Amplitude vs 2σ Doppler-spread

The graphs of peak signal amplitude vs Doppler-spread (Fig. 28) support the conclusions derived from Table 2 but, in addition, show the scatter of the measured values. The merit of this form of presentation is that it graphically illustrates the spatial grouping of the different measurement sets on the amplitude—Doppler-spread plane. The measurements of Experiment 27 (Fig. 28(a)), which correspond to reflection from an undisturbed daytime ionosphere, occupy a region of the graph corresponding to strong signals with very small Doppler-spreads. By contrast, the measurements of Experiment 47, corresponding to magnetically disturbed, daytime, subauroral conditions, are seen to occupy a region of small amplitudes and large Doppler-spreads. Their amplitudes are on the order of 10 to 15 dB smaller than those of Experiment 27 and their Doppler-spreads are approximately two orders of magnitude greater. Judging from their smaller amplitudes and wider Doppler-spreads, we surmise that these are primarily scattered signals from an irregular ionosphere. The third signal group in Fig. 28(a) represents the results of Experiment 48, the post-perturbation, subauroral, daytime measurements. The signals in this group are characterized by large signal amplitudes and moderate Doppler-spreads. The ionogram for this experiment (Fig. 18(c)) has the characteristics of a classic range-spread spread F ionogram. The measured peak signal amplitudes for Experiment 48 are on the order of 20 dB higher than those of Experiment 47, but their Doppler-spreads are roughly an order of magnitude smaller. In comparison with the measurements of Experiment 27, those of Experiment 48 indicate a somewhat larger amplitude and a Doppler-spread that is roughly an order of magnitude larger. The interpretation of the measurements of Experiment 48 is that they correspond to multipath reflection from a strong but irregular ionospheric medium in which the drift (and turbulent) velocities are smaller than during magnetically disturbed periods.

A small subgroup of the measured points of Experiment 47 have amplitudes approaching those of Experiment 27 and are responsible for raising its average signal level in Table 2. These points refer to signals received on a single frequency (2.8 MHz) that are most likely multipath-reflected signals. Their amplitudes put them in the class of reflected signals, but their large Doppler-spreads imply reflection from an irregular medium under conditions of magnetic disturbance. As seen in Section 5.2, their delay-spreads are consistent with those of signals for Experiment 48, which supports their identification as multipath reflections.

The nighttime measurements of Fig. 28(b) consist of Experiments 31 and 33 for quiet magnetic conditions (Fig. 13(a)) and Experiments 53 and 56 for disturbed magnetic conditions (Fig. 19(a)). Conditions during Experiments 31 and 33 differed in that the propagation path during Experiment 31 was subauroral while that for Experiment 33 lay on the oval-trough boundary. The result of the different propagation path locations appears to be a roughly 10 dB difference in signal level with the higher level obtained on the subauroral path. Their Doppler-spreads are within a factor of two of one another and are consistent with those obtained during the daytime, post-perturbation measurements of Experiment 48. Their amplitude differences can be explained in terms of a multipath-reflection process for Experiment 31 and a scattering process for Experiment 33. The larger value of Doppler-spread for Experiment 31 (approximately a factor of 2) is attributed to the fact that its signal consists of two distinct returns that differ in mean Doppler shift by approximately 4 Hz (Fig. 24).

The measurement points corresponding to magnetically disturbed, nighttime, auroral conditions (Experiments 53 and 56) occupy a region on Fig. 28(b) that is comparable to that of Experiment 47, their daytime subauroral counterpart, on Fig. 28(a). The Doppler-spread of these measurements is roughly an order of magnitude larger than those of the quiet nighttime measurements. Their peak signal amplitude values are roughly equivalent to those of Experiment 33, the magnetically quiet, nighttime, auroral measurements, and approximately 15 to 20 dB smaller than those of Experiment 31, the magnetically quiet, nighttime, subauroral measurements.
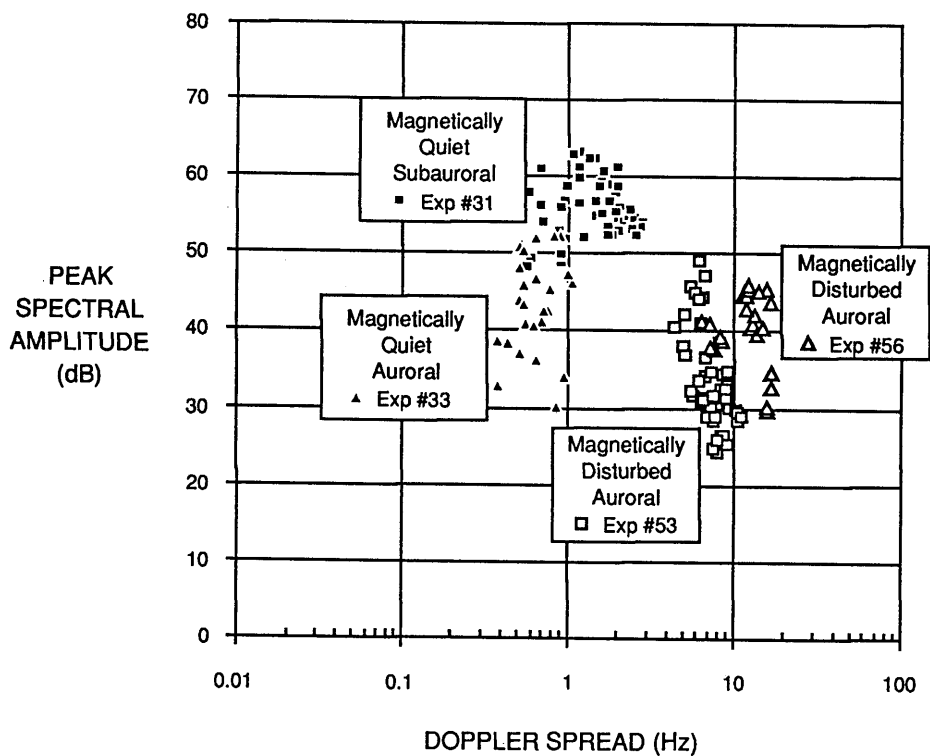
5.2 Scatter Plot of Peak Signal Amplitude vs 2σ Delay-spread

For simply-reflecting channels, delay-spread is predominantly influenced by the normal dispersive effects of the ionospheric medium, while for scatter channels, delay-spread is frequently more strongly influenced by the spatial dispersion of the scatterers. For these reasons, delay-spread does not appear to be simply related to the degree of ionospheric disturbance, as was the case with the Doppler-spread. This difference is reflected in the absence of a clear separation in Fig. 29 of the different signal groups representing signal amplitude vs delay-spread.

The effect of normal ionospheric dispersion is clearly illustrated in Fig. 29(a), where the simply-reflected, daytime signal (Experiment 27) shows a roughly uniform dispersion of delay-spread over approximately two orders of magnitude (note the diminution of signal amplitude with increasing delay-spread). Daytime multipath channels, which are subject to the effects of both a distributed reflecting medium and of normal ionospheric dispersion, manifest both influences. Thus, the points representing Experiment 48 in Fig. 29(a) are tightly bunched into two distinct groups of points. The group with the smaller average delay-spread is representative of frequencies that are well below the F layer critical frequency (see Fig. 18(c)). The primary contribution to the delay dispersion at these frequencies is the spatial distribution of the reflectors, with the result that the minimum delay-spread of this group is more than an order of magnitude greater than that of the simply-reflected signals of Experiment 27. The second group of points, corresponding to frequencies at or near the F layer critical frequency, are significantly affected by the large dispersive effects at or near that layer as well as by the spread due to the spatial distribution of reflectors. As a result, the mean delay-spread for these points is larger, by roughly an order of magnitude, than that of the first group of points. Finally, the scatter signals of Experiment 47 are reasonably tightly grouped except for a small group of signals whose amplitudes and delay-spreads tend towards those of Experiment 48. This group of points consists of signals whose frequencies are well below the F layer critical frequency and contain,
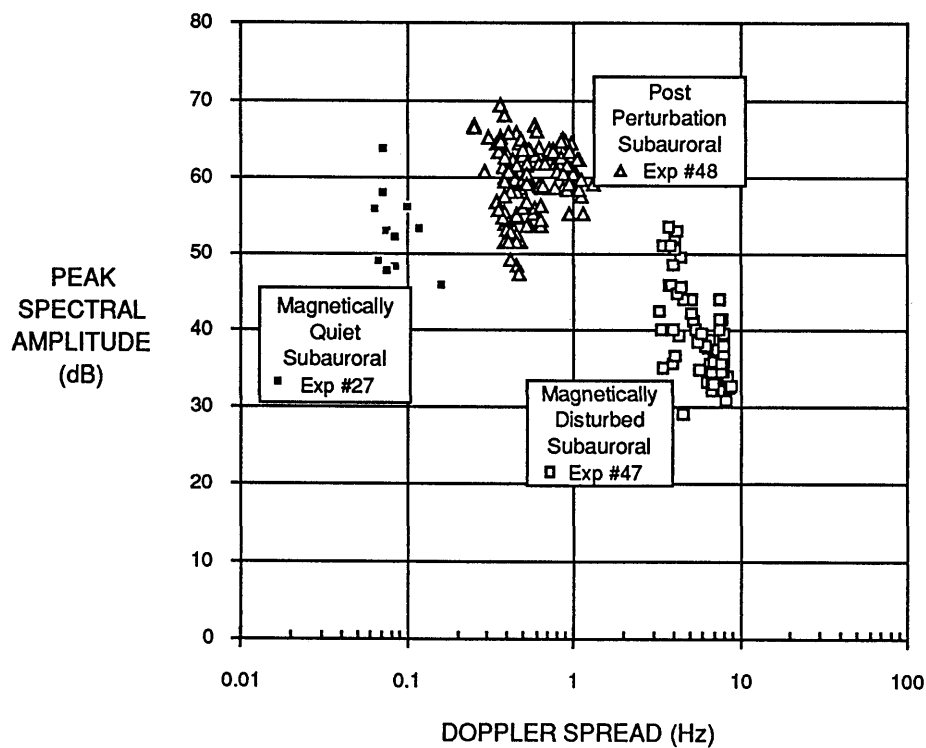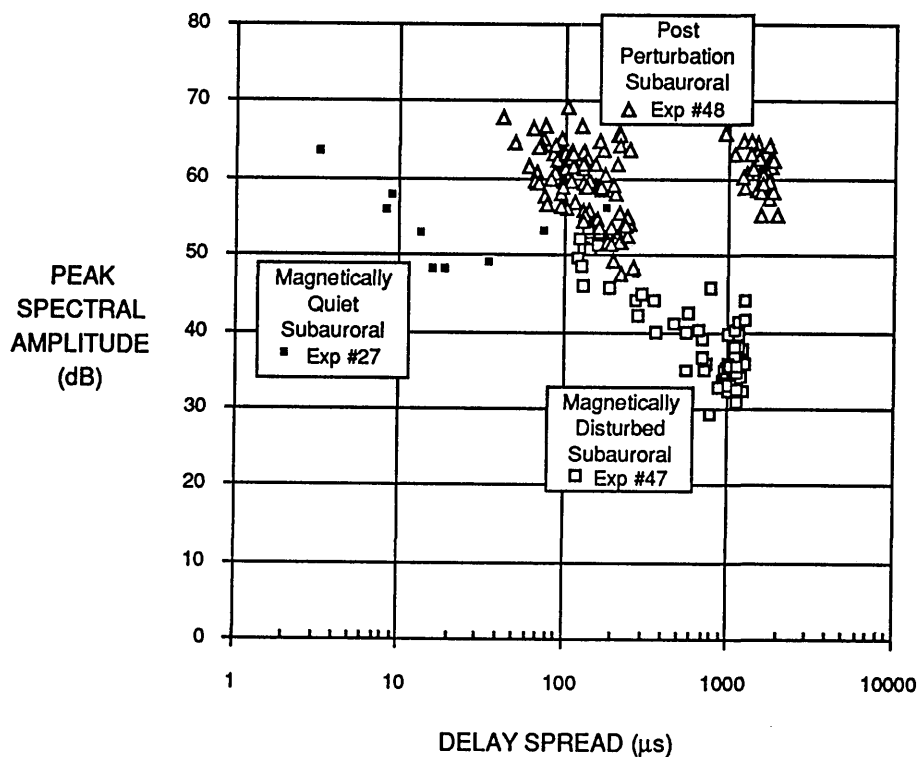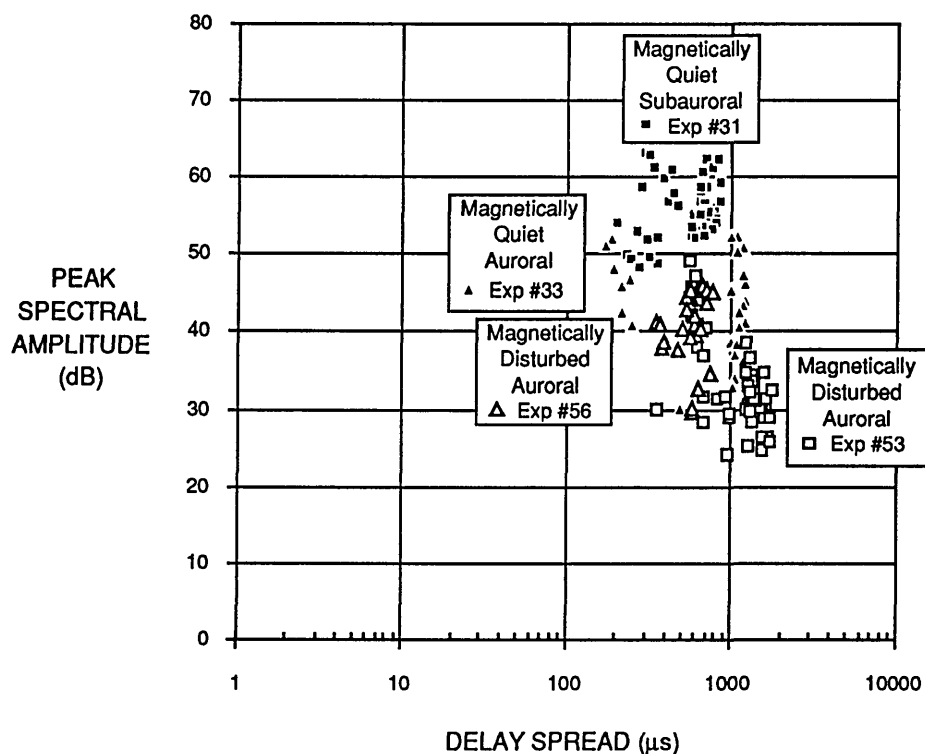
(a) Daytime measurements

(b) Nighttime measurements

Fig. 28 — Scatter plot of peak signal amplitude vs 2σ Doppler-spread

(a) Daytime measurements

(b) Nighttime measurements

Fig. 29 — Scatter plot of peak signal amplitude vs 2σ delay-spread

or are dominated by, multipath reflections as described in Section 5.1. The presence of the multipath reflections among the scattered signals causes their amplitude and delay-spread characteristics to approach those of the purely multipath returns of Experiment 48.

The delay-spread behavior of the nighttime signals also differs depending on the degree of magnetic disturbance and the location of the path midpoint relative to the auroral oval. Oval measurements made during magnetically disturbed periods tend to be tightly grouped, as can be seen in Fig. 29(b) (Experiments 53 and 56), while those made during magnetically quiet conditions are split into two groups (Experiment 33). Of the two measurement groups in Experiment 33, one group exhibits smaller delay-spreads than does the magnetically disturbed cases, while the second group exhibits delay-spreads comparable to those of the magnetically disturbed cases. The behavior of delay-spread for Experiment 33 is very similar to that of Experiment 48, the post-perturbation daytime measurement. The property that these two cases have in common, which contributes to the similarity in the distribution of their measured delay-spreads, is the range-spread character of their F layer ionogram traces. In each case, the slope of the range-spread trace is small and constant for most frequencies, but steepens sharply as the frequency approaches the layer critical. The steepening of the slope of the ionogram trace results in enhanced delay dispersion for frequencies near the layer critical frequency.

The nighttime, subauroral measurements during quiet magnetic conditions (Experiment 31) tend to be dispersed uniformly over an extended interval, in a manner similar to that of Experiment 27, implying that ionospheric dispersion is a controlling factor. The delay-spreads, however, are much larger than for Experiment 27, which is most likely associated with the presence of the delayed sidescatter signal in the case of Experiment 31.

5.3 Scatter Plot of Peak Signal Amplitude vs Spread Factor

Spread factor is a fundamental parameter for characterizing the distortion properties of a communication channel. As previously indicated, it is defined as the product of the 2σ delay-spread with the 2σ Doppler-spread, and as such it incorporates both the bandwidth coherence and the time coherence properties of the channel. For these reasons, it is important to characterize the measurements on the high-latitude NVIS channel in terms of this parameter. Figure 30 is a scatter plot of peak signal amplitude vs spread factor. Because of its dependence on delay- and Doppler-spread, the graph of Fig. 30 has properties that are a combination of those of Figs. 28 and 29. The most important features retained by Fig. 30 are (1) that spatial separation of measured signal points is maintained for the various groups examined in this case, (2) that the range of the spread factors is approximately five orders of magnitude (10^{-7} to 10^{-2}) from the best to the worst channel conditions, and (3) that the range of signal amplitudes is on the order of 45 dB from the weakest scatter signal to the strongest reflected signal.

6. SUMMARY AND CONCLUSIONS

Propagation mechanisms supported by high-latitude channels include simple reflection from a smooth, laminar ionosphere, and multipath-reflection, scattering, or a combination of the two from an irregular ionosphere. High-latitude channels supporting simply-reflected signals have characteristics (amplitude, delay- and Doppler-spreads) that are comparable with those observed on a quiescent midlatitude channel. Channels supporting multipath-reflection mechanisms typically have peak signal amplitudes that are comparable with those of the simple reflection channels but have delay- and Doppler-spreads that are approximately an order of magnitude larger. Scatter channels have amplitudes that are, on average, two orders of magnitude smaller than those reflected signal channels

DAYTIME MEASUREMENTS

(a) Daytime measurements
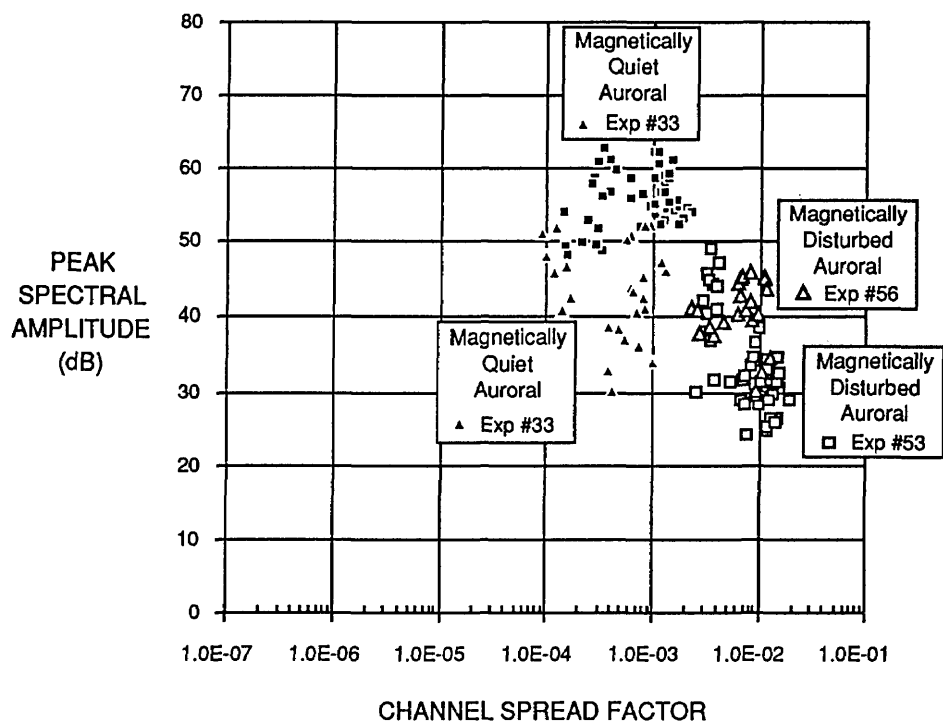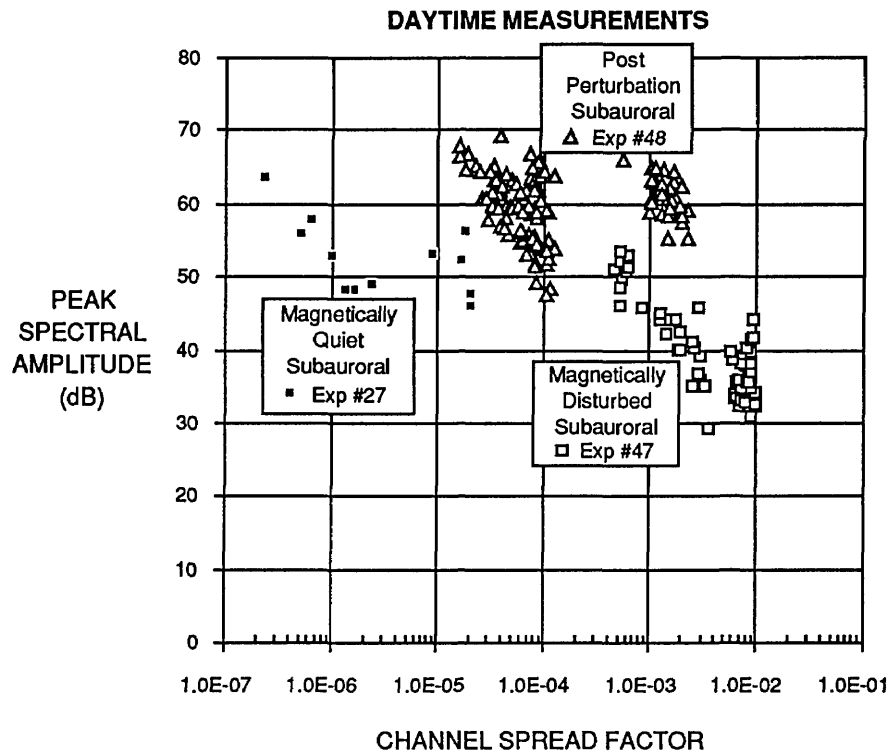

(b) Nighttime measurements

Fig. 30 — Scatter plot of peak signal amplitude vs spread factor

(simple or multipath-reflection) and delay- and Doppler-spreads that are approximately two orders of magnitude larger than those of simple reflection channels.

Results from this series of NVIS HF propagation experiments show that conditions on the high-latitude channel can vary widely depending on the degree of magnetic disturbance and on the location of the propagation path relative to the auroral oval. The following observations have been made:

1. Magnetically quiet, subauroral paths generally encounter quiescent ionospheric conditions and a simple reflection channel as in the case of the daytime measurements of Experiment 27 in this report. If, however, the path comes in close proximity with the nighttime auroral oval, as in the case of Experiment 31, then effects due to irregularities in the overhead ionosphere or the adjacent oval region may be observed in spite of the absence of magnetic activity. The presence of irregularities in the medium results in a channel whose characteristics resemble those of a multipath-reflection channel.

2. An isolated magnetic disturbance on a daytime, subauroral path can lead to irregular conditions in the overhead ionosphere causing radio blackout, as in the case of Experiment 46, and severe spread F and a scatter channel, as in the case of Experiment 47. Post-perturbation effects involving range-spread spread F and a multipath reflection channel may persist for several hours after the magnetic perturbation, as in the case of Experiments 48 to 50.

3. Auroral path measurements in this series of experiments invariably encountered irregular ionospheric conditions (scatter channels) independent of the degree of magnetic disturbance (e.g., Experiments 33, 53, and 56). The major difference noted in channel characteristics between magnetically quiet and magnetically disturbed auroral conditions was in the extent of the Doppler-spread, which was approximately an order of magnitude larger for the magnetically disturbed case.

4. Scatter channels observed on subauroral paths during magnetically disturbed daytime conditions exhibited the same amplitude and delay- and Doppler-spread characteristics as were observed for scatter channels on magnetically disturbed auroral paths.

5. For paths that traverse the ionospheric D layer within the region of the diffuse aurora, such as the NVIS path discussed in this report, strong magnetic activity ($K > 3$) is usually accompanied by periods of radio blackout.

Results consistent with these were observed on a 1300 km high-latitude path between Sondrestrom, Greenland and Keflavik, Iceland (Wagner et al. 1993; Wagner et al. 1995). The midpoint of the Greenland-Iceland propagation path was at a corrected geomagnetic latitude of 72° as contrasted with a CGL of 65° for the current path. Because of its higher latitude location, the Greenland-Iceland path was within the auroral oval for a larger fraction of each day, but never traversed the diffuse auroral region.

ACKNOWLEDGMENTS

REFERENCES

Bates, H.F. and R.D. Hunsucker. 1974. "Quiet and Disturbed Electron Density Profiles in the Auroral Zone Ionosphere," *Radio Sci.* **9**(4), 455-467.

Bello, P.A. 1963. "Characterization of Randomly Time Variant Linear Channels," *IEEE Trans. Communicat. Systems* **CS-11**(4), 360-393.

Buchau, J., B.W. Reinisch, E.J. Weber, and J.G. Moore. 1983, "Structure and Dynamics of the Winter Polar Cap F Region," *Radio Sci.* **18**(6), 995-1010.

Buchau, J., E.J. Weber, D.N. Anderson, H.C. Carlson, J.G. Moore, B.W. Reinisch, and R.C. Livingston. 1985. "Ionospheric Structures in the Polar Cap: Their Origin and Relation to 250 MHz Scintillation," *Radio Sci.* **20**(3), 325-338.

Feldstein, Y.I. 1966. "Peculiarities in Aurora and Magnetic Disturbances Distribution in High Latitudes," *Planet. Space Sci.* **14**, 121-130.

Feldstein, Y.I. and G.V. Starkov. 1967. "Dynamics of Auroral Belt and Polar Geomagnetic Disturbances," *Planet. Space Sci.* **15**, 209-229.

Hartz, T.R. and N.M. Brice. 1967. "The General Pattern of Auroral Particle Precipitation," *Planet. Space Sci.* **15**, 301-329.

Heelis, R.A. 1982. "The Polar Ionosphere," *Revs. of Geophys. and Space Phys.* **20**(3), 567-576.

Hunsucker, R.D. 1992. "Auroral and Polar-cap Ionospheric Effects on Radio Propagation," *IEEE Trans. Antennas Propagat.* **40**(7), 818-828.

Knudsen, W.C. 1974. "Magnetospheric Convection and the High-latitude F2 Ionosphere," *J. Geophys. Res.* **79**(7), 1046-1055.

Robinson, R.M., R.T. Tsunoda, J.F. Vickrey, and L. Guerin. 1985. "Sources of F Region Ionization Enhancements in the Nighttime Auroral Zone," *J. Geophys. Res.* **90**(A8), 7533-7546.

Muldrew, D.B. 1965. "F Layer Ionization Troughs Deduced from Alouette Data," *J. Geophys. Res.* **70**(11), 2635-2650.

Sharp, G.W. 1966. "Midlatitude Trough in the Night Ionosphere," *J. Geophys. Res.* **71**(5), 1345-1356.

Spiro, R.W., R.A. Heelis, and W.B. Hanson. 1978. "Ion Convection and the Formation of the Mid-latitude F Region Ionization Trough," *J. Geophys. Res.* **83**(A9), 4255-4264.

Stein, S. 1987. "Fading Channel Issues in System Engineering," *IEEE J. on Selected Areas in Communication* **SAC-5**(2), 68-89.

Tsunoda, R.T. 1988. "High Latitude F Region Irregularities: A Review and Synthesis," *Revs. of Geophys.* **26**(4), 719-760.

Wagner, L.S. and J.A. Goldstein. 1985. "High Resolution Probing of the HF Skywave Channel: F2 Layer Results," *Radio Sci.* **20**(3), 287-302.

Wagner, L.S., J.A. Goldstein, and W.D. Meyers. 1988. "Wideband Probing of the Transauroral Channel: Solar Minimum," *Radio Sci.* **23**(4), 555-568.

Wagner, L.S. and J.A. Goldstein. 1991. "Response of the High Latitude HF Skywave Channel to an Isolated Magnetic Disturbance," *Proc. of Fifth International Conf. on HF Radio Systems and Techniques,* 233-237, IEE, Edinburgh.

Wagner, L.S., J.S. Goldstein, M.A. Rupar, and E.J. Kennedy. 1993. "Northern Exposure 92: An Investigation of Transauroral HF Radio Skywave Propagation," NRL Report NRL/FR/5554--93-9575.

Wagner, L.S., J.S. Goldstein, M.A. Rupar, and E.J. Kennedy, "Delay, Doppler, and Amplitude Characteristics of HF Signals Received Over a 1300-km Transauroral Skywave Channel," (accepted for publication in *Radio Science*; estimated pub'n **30**(3), May-June 1995).

Weber, E.J. and J. Buchau. 1981. "Polar Cap F Layer Auroras," *Geophys. Res. Lett.* **8**, 125-128.

Whalen, J.A. 1970. "Auroral Oval Plotter and Nomograph for Determining Corrected Geomagnetic Local Time, Latitude, and Longitude for High Latitudes in the Northern Hemisphere," *AFCRL-70-0422, Environmental Research Papers No. 327,* AD 713170.

Whalen, J.A. 1985. "The Aurora," *Handbook of Geophysics and the Space Environment,* A.S. Jursa editor, Ch. 12, ADA 167000, NTIS.

Appendix
DESCRIPTION OF THE NRL CHANNEL PROBE

The NRL HF Channel Probe is a wideband, bistatic, time domain channel sounder developed at NRL for the purpose of investigating the wideband properties of the HF skywave channel at a signal bandwidth of 1 MHz. A certain amount of bandwidth flexibility was built into the probe design to broaden the range of applications for which it would be suited. Over time, the operational properties of the probe were extended to allow greater flexibility in how data could be collected.

The basic probe measurement is a complex pulse response of the radio channel. The measurement is done sequentially at a number of frequencies. System bandwidths available at experiment start time are 31.25 kHz, 125 kHz, 250 kHz, and 1 MHz, corresponding to probe pulsewidths of 32 μs, 8 μs, 4 μs, and 1 μs. The frequencies and system bandwidths are selected by the operator at the start of each experiment. The bistatically configured transmitter and receiver are programmed to step through identical frequency tables synchronously. Repeated measurements at each frequency, prior to stepping to the next frequency, are required for observing fast fluctuations of a received signal. The sampling interval of repeated pulse response measurements is variable and supports unambiguous Doppler windows ranging between ±0.8 and ±2.2 Hz in our standard operating format and between ±7.7 and ±30.6 Hz in our extended Doppler format.

The system uses a spectrum spreading coded modulation at the transmitter that is "de-spread" at the receiver in a fast, real-time correlation-processor to produce the effect of a short-pulse sounding signal. The coded modulation is a continuously repeated, maximal length, pseudo-random noise (PRN) binary sequence that biphase modulates the transmitter carrier. Two PRN sequences are available, one of 255 chips and a second of 2047 chips, supporting narrow and wideband operation, respectively. The duration of the 255 chip sequence is 8.16 ms corresponding to a chip rate and system bandwidth of 31.25 kHz. The duration of the 2047 chip sequence is 8.188 ms corresponding to a chip rate and system bandwidth of 250 kHz. A 25% duty factor pulse modulation, superimposed on the biphase modulated carrier, can be used to expand the basic system bandwidths of 31.25 kHz and 250 kHz to 125 kHz and 1 MHz, respectively.

Figure A1 is a block diagram of the channel probe instrument. Time synchronism and phase coherence between transmitter and receiver are assured by the presence of very stable and accurate frequency and time sources at both sites. The frequency standard at the transmitter site is a cesium beam reference oscillator, while that at the receiver is a rubidium vapor resonance oscillator. Clock synchronization is established at transmitter and receiver sites to a relative time accuracy of better than 10 μs using either LORAN-C, GPS broadcast time, or a combination of the two.

The transmitter signal is generated from a phase-stable reference, at a frequency of 39.5 MHz, which is biphase modulated by the PRN sequence. The signal is then optionally pulse modulated to introduce a 4:1 bandwidth expansion, amplified, down-converted to the appropriate HF frequency, filtered, and delivered to the linear power amplifier and the antenna. All oscillators are locked to the station frequency-standard.
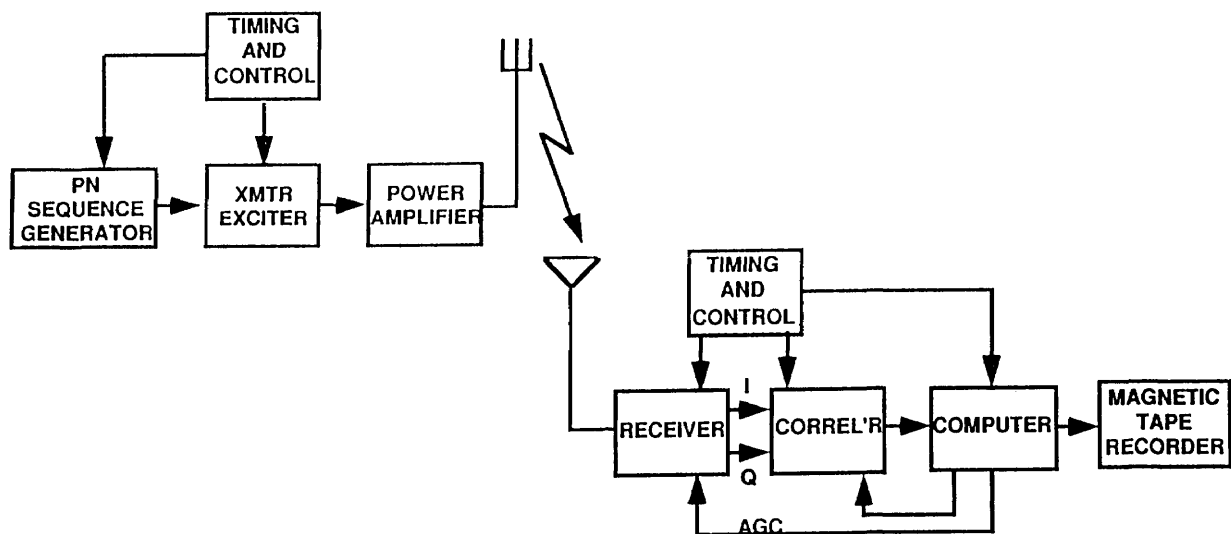
Fig. A1 — Channel probe block diagram

The radio receiver is a phase-stable heterodyne receiver with computer controlled i-f gain and local oscillators locked to the station frequency-standard. The output of the i-f amplifier is converted to in-phase (I) and quadrature-phase (Q) baseband video components, which are filtered, amplified, and converted to a 12 bit digital representation of the received signal(s). The digitized signals are then passed to a real-time correlator unit for cross-correlation with a series of delayed replicas of the transmitted PRN sequence, thereby producing a sampled representation of the channel pulse response. The sampled data output of the correlator is then passed to the system computer for further screening, disk storage, and eventually to magnetic tape for permanent storage.

The start of a measurement, specified to a resolution of one minute, is precisely controlled by an automatic "clockstart" strobe at each site. Thereafter, experiment synchronization is maintained using extremely accurate clock pulse generators to "event-control" the microprocessors at the two locations. Frequency tables and all other experiment parameters are controlled by the microprocessors that have been preset by the operator with identical frequency and parameter tables.

Channel probe operation is flexible since the operating format is software- or firmware-controlled. Standard operating procedure usually consists of an initial narrowband "sounder" run that makes a single pass, in relatively fine frequency steps, through the range of frequencies supported by the ionosphere. The purpose of this run is to collect data for an ionogram and also to locate those delay intervals that are occupied by the various propagating ionospheric modes. The sounder mode is followed by an extended period of probing (prober mode), which can be narrowband (255 chips) or wideband (2047 chips).

During standard prober mode operations, repeated pulse response measurements are made on a limited set of frequencies of interest. In cases where interest is in the relatively slow ionospheric changes associated with the passage of an acoustic gravity wave or traveling ionospheric disturbance (TID), a round-robin format is used in which a single pulse response measurement is made on each frequency in turn. In cases where one is interested in more rapid fluctuations, it is necessary to dwell at each frequency while making repeated pulse response measurements, prior to proceeding to the next frequency.

In the set of prober measurements discussed in this report, the narrowband format (255 chips; bandwidth = 31.25 kHz) was used predominantly. Since the auroral channel is generally a rapidly varying one, and since interest was centered on examining the scattering function of the channel, an operational format consisting of extended dwells at each frequency was used. The pulse response measurement repetition rate (the data sampling rate) was adjusted according to the anticipated signal Doppler-spread. The time interval devoted to the prober mode was approximately 14 minutes for each experiment.

The duration of the ionogram data collection period was approximately 40 seconds. The ionogram data collection period preceded the probing period by 15 minutes to allow time for evaluating channel conditions and for deciding on the "best" set of parameters given the ionospheric conditions. Since conditions on the auroral channel can change violently in a short period of time, this procedure did not always result in the optimum format for the given conditions.